Enhanced Electrical, Optical and Chemical Properties of Graphene Oxide through a Novel Phase Transformation

by

Priyank Vijaya Kumar

B.Tech. Metallurgical and Materials Engineering, Indian Institute of Technology Madras, 2010

Submitted to the Department of Materials Science and Engineering
in partial fulfillment of the requirements for the degree of

DOCTOR OF PHILOSOPHY IN MATERIALS SCIENCE AND ENGINEERING

AT THE

MASSACHUSETTS INSTITUTE OF TECHNOLOGY

June 2015

Signature redacted

Signature of Author: _____
Department of Materials Science and Engineering
May 13th, 2015

Signature redacted

Certified by: _____
Jeffrey C. Grossman
Professor of Materials Science and Engineering
Thesis Supervisor

Signature redacted

Accepted by: _____
Donald R. Sadoway
John F. Elliott Professor of Materials Science and Engineering
Chair, Departmental Committee on Graduate Students

Enhanced Electrical, Optical and Chemical Properties of Graphene Oxide through a Novel Phase Transformation

Priyank V. Kumar

B. Tech., Metallurgical and Materials Engineering
Indian Institute of Technology Madras, India, 2010

Submitted to the Department of Materials Science and Engineering
in partial fulfillment of the requirements for the degree of

DOCTOR OF PHILOSOPHY
Materials Science and Engineering
Massachusetts Institute of Technology

Advisor: Prof. Jeffrey C. Grossman

Committee members:
Prof. Angela Belcher
Prof. Alfredo Alexander Katz

May 22, 2015

Contents

Acknowledgements

Pursing a PhD had been my dream; and without others, it would have remained one.

I take this opportunity to thank all those who have made this dream a reality through their selfless efforts, support and encouragement.

First and foremost, I would like to thank my thesis supervisor, Prof. Jeffrey C. Grossman (Jeff), who has been a truly shaped my professional and personal development. He has made me feel really comfortable in the group and has given me utmost flexibility to pursue what I liked. His passion for research, desire to solve important problems and most importantly, his attitude towards students and his friendly nature has helped me enjoy and value my PhD experience. I thank him for keeping faith and allowing me to learn both computational and experimental techniques during my PhD.

With Jeff (a.k.a. Jammin' Jeff), work doesn't happen without fun. I am not sure whether to thank him for picking on me to ask the first question during our group meetings with his majestic Sheriff hat, but that did make me pay utmost attention to every single talk during our group meetings. My imitation of Jeff during first year did pose a mild threat to my PhD, when Jeff got so delighted he actually promised the group to keep me beyond five years. He sometimes introduced me as a 'visiting student' to the group, for reasons only known to him and others in the group, which did scare me a bit.

Overall, I have learnt a lot from Jeff and I consider it a blessing to have been his student. He has, is and will remain an inspiration to me. I wish him the best for the future.

I'm grateful to my committee members, Prof. Angela Belcher and Prof. Alfredo Alexander Katz, who have taken significant time to assess my work and provide valuable suggestions. I thank Prof. Belcher for giving me access to experimental facilities, which proved to be immensely helpful during my PhD.

Next, I would like to thank all the Grossman group members (former and current). They have been a family to me. I would like to thank Marco (Prof. Bernardi *et al.*), who was the first person I worked with in the group. His constant support and guidance helped me kick start my PhD. He has been a true inspiration to me. I also thank my former labmates Giuseppe (Pepe), Engin-abi and Rajamani for their great friendship and help during the initial phase of my PhD. My current labmates Can-iko, Kayahan (Kayo) and Sangjin have made my stay in the lab a beautiful experience. I can't thank them enough for all their help during my PhD. Special thanks to Can and Kayo for accompanying me during lunch and dinner. I'll cherish all those moments for years to come. I also extend thanks to all current members of the group. They have been super fun to work with. I have had memorable moments with them and they have helped me ease through the final phase of my PhD.

I want to thank Donghun, who joined the group along with me. He has been a great friend and an awesome person to discuss research and life with. I will never forget those days when we studied together for midterm/qualifying exams and our periodic lunch/coffee

session discussions. I thank Jeong Yun, who has been so kind and has helped me on so many occasions during my PhD. I was fortunate to graduate along with her. Without her support, I couldn't have completed my thesis on time.

I thank Neelkanth (Neel), who has been a good friend and a mentor when it came to experiments. Being a busy PhD student himself, he worked hard to help me acquire significant experimental knowledge and has been a significant part of my research. His constant availability and motivation to tackle important problems has been truly inspiring. My work would have been incomplete without Guan-Yu (Prof. Chen now), who has shared common interests and has given me wonderful collaborative opportunities.

I want to thank Aravind (Anna), Ketan and Deepak, who have been great friends since my undergrad. My long discussions with Aravind and Ketan over countless coffee/lunch/dinner sessions about research specifics and the "big picture" that one's research needs to address have helped me assess my own research. They have been really fun to hang out with. I thank Julius, Abraham and Michael for being great roommates.

My last two years at MIT were spectacular, thanks to the MIT cricket club, which helped me nurture my passion for cricket. I wish to thank all the members in this club, who have given me such great company on and off the field. I also wish to thank people at the badminton club who have been a great bunch to spend evenings with. A lot of new friends made with these clubs and so many wonderful memories to cherish!

I thank my parents, my brother, my sister-in-law, Aadrith and all other family members who have been extremely supportive and caring throughout my PhD. A lot of inspiration from my parents and my brother has kept me moving through my PhD and I look up to them. I want to thank Tiziana, a charming Italian girl I met during the first year of my PhD - she has made my PhD experience a special and memorable one. I am indebted to her support, love and companionship. I thank her parents for their utmost care whenever I visited them in Italy.

Abstract

Graphene oxide (GO) is a versatile, solution-processable candidate material for next-generation, large-area, ultrathin electronics, optoelectronics, energy conversion and storage technologies. GO is an atom-thick sheet of carbon functionalized with several oxygen-containing groups dominated by the epoxy and hydroxyl functional groups on the basal plane, with carboxyls and lactols at the sheet edges. It is well known that reduction of GO at temperatures $> 150°C$ leads to the removal of oxygen atoms from the carbon plane, leading to the formation of reduced GO (rGO) structures. Although GO has been utilized for multiple applications in the last decade, our understanding of the structure-property relationships at the atomic-level has still been lacking owing to the amorphous nature and chemical inhomogeneity of GO, which has in turn limited our ability to design and tailor GO nanostructures for high-performance applications. In particular, the material's structure and its structural evolution at mild annealing temperatures ($< 100°C$) has been largely unexplored.

In this thesis, we use a combination of first-principles computations, classical molecular dynamics simulations based on reactive force fields and experiments to model realistic GO structures and develop a detailed understanding of the relationship between the carbon-oxygen framework and the sheet properties, at the atomic level. Based on our understanding, we demonstrate a new phase transformation in GO sheets at mild annealing temperatures (50-80°C), where the oxygen content is preserved and as-synthesized GO structures undergo a phase separation into

prominent oxidized and graphitic domains facilitated by oxygen diffusion. Consequently, as-synthesized GO that absorbs mainly in the ultraviolet region becomes strongly absorbing in the visible region, photoluminescence is blue shifted and electronic conductivity increases by up to four orders of magnitude. We then use this novel phase transformation to improve two sets of applications. 1) We demonstrate that cell capture devices making use of phase transformed-GO substrates have higher capture efficiencies compared to devices making use of as-synthesized GO substrates. 2) We show that the reduction of phase transformed-GO leads to better electrical properties of rGO thin films. Our results fill an important gap and establish a complete theory for structural evolution of GO over the entire range of temperatures, i.e. from room temperature to $\sim$1000°C. Taken together, this structural transition in GO enables us to predict and control the sheet properties in new ways, as opposed to reduction, which is till date the only handle to control the structure of GO. This could potentially open the door for completely new applications or for enhancing the performance of existing applications based on GO.

Chapter 1

Introduction

1.1 What is graphene oxide?

In order to answer this question, one needs to first understand a particular material that has revolutionized the fields of physics and materials science in the last decade. This material is called graphene, which is a two-dimensional (2D) monolayer form of carbon arranged in a hexagonal lattice (Figure 1.1a) [1]. Its discovery has impacted technologies ranging from electronic and optoelectronic applications at the nanoscale all the way up to membrane and mechanical applications at the macroscale [2]. This has been possible because of a rare combination of exotic electrical, optical and mechanical properties in this atomically thick nanomaterial. For instance, the electronic mobility of suspended graphene is 10^5-10^6 $cm^2V^{-1}s^{-1}$ at room temperature, compared to 10^3 $cm^2V^{-1}s^{-1}$ in silicon, a semiconductor material we come across in everyday life [3]. Similarly, the ultimate tensile strength of graphene is 100,000 MPa, compared to 400 MPa for steel, which is a common structural material [3].

While various experiments have already demonstrated unusual fundamental physics and sheet properties of graphene [2], and have translated them into proof-of-concept devices [4], its large-scale fabrication has been a major hurdle toward its commercial success [5]. Mechanical exfoliation and chemical vapor deposition have remained popular methods to produce graphene and have been useful to perform fundamental experiments [6]. In the former, a simple scotch-tape procedure is used to peel single layers of graphene from graphite, while in the latter, a carbon source (for ex. methane gas) is typically used as a precursor in a high-temperature chamber to deposit graphene on a suitable substrate (for example, copper) [7]. Both these methods produce high quality graphene (in terms of materials properties), however, these methods are limited to small-scale fabrication (up to a few centimeters) [8].

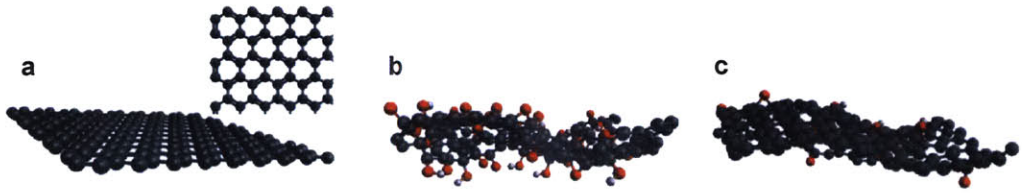

Figure 1.1: Atomic structures. (a) Honeycomb lattice of monolayer graphene. (b) Structure of graphene oxide (GO) showing the distortions in graphene lattice induced by oxygen (sp^3) functionalization. (c) Structure of a reduced GO (rGO) monolayer showing restoration of graphitic structure through the removal of a large fraction of oxygen atoms from GO. Carbon, oxygen and hydrogen atoms are represented by black, red and grey spheres, respectively.

1.1.1 Solution synthesis of graphene

In order to overcome this issue, Ruoff and co-workers used a solution-based approach to produce graphene monolayers and thin-films, termed as the chemical

exfoliation method (Figure 1.2) [9, 10]. In this approach, graphite undergoes a redox reaction forming an oxidized form of graphite, called graphite oxide. Once oxygen binds to individual graphene layers, the Van der Waals forces holding together the graphene sheets are weakened. As a result, when graphite oxide is introduced in a solvent (typically, water), the layers readily exfoliate and form single layers of graphene, albeit now functionalized with oxygen atoms (Figure 1.1b). These single layers of oxygen-functionalized graphene are termed as graphene oxide (GO). Deposition of such monolayers on to suitable substrates is readily achieved through spin coating or drop casting [11]. In order to obtain graphene sheets, removal of oxygen atoms is crucial keeping the carbon framework in tact. A large fraction of the covalently bonded oxygen atoms are removed through thermal or chemical reduction means to obtain graphene or reduced GO (rGO) sheets (Figure 1.1c). These rGO sheets inevitably contain residual oxygen due to thermodynamic limitations toward complete removal of oxygen atoms, which will be discussed later in this thesis [8, 12].

1.2 Why are we interested in GO?

While graphite oxide was first produced in 1859 by a chemist named Benjamin Brodie [13] and its synthesis procedures have been improved over the last century, this material has gained rising popularity only since 2006. This is mainly due to two reasons:

1. The potential it holds for the large-scale production of graphene, which requires efficient removal of oxygen atoms from the GO sheets.

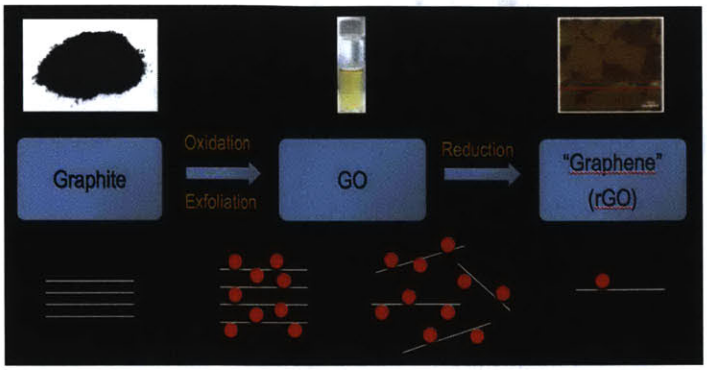

Figure 1.2: Schematic depicting the solution-based approach to produce graphene monolayers through oxidation of graphite followed by exfoliation in water and subsequent reduction. Graphite powder, straightforward suspension of GO in water and deposition of monolayers of rGO are shown in the top panel. The bottom schematic elucidates the structural changes taking place during the entire process, with green straight lines representing monolayers of graphene and the red circles representing the oxygen atoms bonded to the graphene plane.

2. The inherent functionality embedded in GO sheets due to the presence of a rich oxygen framework, which makes GO attractive for its own characteristics. This requires keeping the oxygen atoms intact and utilizing their presence effectively [6].

The utilization of GO in devices has many advantages. Production of GO using the widely available Hummers' method is solution-based, straightforward and inexpensive [6]. Further, GO monolayers can be easily processed in solution, allowing precise control over the number of deposited GO layers, down to a monolayer. These distinct advantages have made GO a versatile candidate for multiple applications including next-generation large-area ultra-thin electronics [14, 5], optoelectronics [6, 15], filtration and separation systems [16, 17, 18], energy conversion and storage technologies [19, 20, 21, 22].

1.3 Structures of as-synthesized GO and rGO

The most commonly accepted structural model of GO is that of a sheet of graphene functionalized with several oxygen-containing groups dominated by the epoxy and hydroxyl functional groups on the basal plane, with carboxyls and lactols at the sheet edges (Figure 1.3a) [23]. Thus, GO contains a mixture of sp^2- and sp^3-hybridized carbon atoms. The defining character of GO is its amorphous nature and chemical inhomogeneity, which have posed difficulties in understanding its exact structure till date [24, 25]. By this, we mean that the positioning of different oxygen functional groups on the graphene basal plane is random during synthesis and hence the exact structure obtained after synthesis is unpredictable.

Although this is the case, we can define the structure of GO in simple terms using two key variables: 1) the oxygen concentration, and 2) the ratio of epoxy to hydroxyl functional groups. For instance, GO produced using a standard protocol, called the Hummers method, typically contains oxygen concentration in the range 30-35 atomic percent (at%) [26]. Variations in the epoxy to hydroxyl ratios are constantly observed in GO structures and hence a particular value is difficult to quote. A range of values between 0.7-1.3 is generally observed [8].

1.3.1 Structural evolution of GO with thermal annealing

Since the primary interest has been to obtain high-quality graphene sheets, researchers have thoroughly studied the process of oxygen removal from the graphene basal plane, termed reduction. Typically, two methods are used to remove oxygen atoms: 1) Thermal reduction - which uses thermal energy to detach the oxygen atoms bonded to the basal plane [8, 12, 27, 28, 29, 30, 31], and 2) Chemical reduc-

tion which uses reduction agents such as hydrazine (N_2H_4), sodium borohydride ($NaBH_4$) and hydrohalic acids (HI) [5].

Ideally, one would prefer to remove every oxygen atom and retain the continuous sp^2 network of the graphene basal plane in tact after the reduction process. In order to achieve this, understanding the process of oxygen removal in both these methods is critical. The mechanism of oxygen removal during thermal reduction is relatively well understood to that during chemical reduction. This is because currently, a large number of chemicals are employed to remove oxygen functionalities and each have different mechanisms for removing epoxies and hydroxyls, resulting in different oxygen removal efficiencies [27]. Understanding chemical reduction is an interesting topic of research, which is however not in the scope of this thesis.

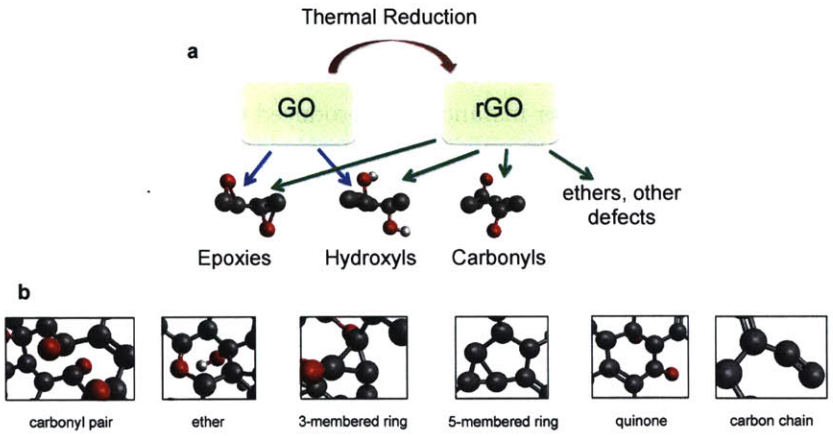

Figure 1.3: Functional groups and defects in GO and rGO. (a) Dominant functional groups present in GO and rGO. (b) Various groups and defects that are created during thermal annealing of GO.

Thermal reduction of GO is a common and straightforward process which can be applied to GO powders, foams, free-standing films and films deposited on a par-

ticular substrate [32]. Typically, GO structures are held at temperatures > 150°C in air or vacuum chambers for 15-60 min to remove oxygen atoms [28]. A number of research groups have studied the mechanism and efficiency of this process at temperatures between 150-1500°C [28]. It is well known that at temperatures greater than 120-150°C, GO sheets begin to lose oxygen and the conversion toward graphene is initiated [28, 33]. As the reduction temperature increases, a greater number of oxygen atoms is removed, thereby restoring a greater fraction of the sp^2 phase in the rGO structures.

However, not all oxygen atoms can be removed from the graphene basal plane even at high temperatures. Typically, the residual oxygen content in rGO (or graphene) sheets is 5-8 at%, which limits the sheet properties from reaching the extraordinary values of graphene obtained by mechanical exfoliation or CVD processes [28, 8]. Experiments and simulations have revealed the formation of highly stable carbonyl and ether groups that hinder the complete reduction of GO to graphene (Figure 1.3) [8]. Further, experiments and theory have shown that carbon atoms are removed from the graphene basal plane during the reduction process in the form of CO and CO_2 molecules [29, 30, 31] . Therefore, the structure of rGO is known to contain carbonyls, ethers, defects such as carbon chains, vacancies (induced by carbon removal) in addition to epoxies and hydroxyls (Figure 1.3b) [8, 34].

1.4 Impact of structural evolution on the sheet properties

The reduction chemistry leads to interesting changes in the rGO structure and provides opportunities for tailoring the sheet properties. As-synthesized GO is insulating (with a sheet resistance of 9 GΩ/sq.) since it contains a large fraction of sp^3-hybridized carbon atoms. Upon reduction, GO undergoes an insulator-semiconductor-semimetal transition due to varying oxygen concentration and the fraction of sp^2/sp^3 hybridized carbon atoms (Figure 1.4b) [35]. The optical absorption and photoluminescence (PL) can be tuned in the visible (Figure 1.4c [36, 37], d), and the carrier mobility can be varied over 9-12 orders of magnitude by altering the oxygen content (and the fraction of sp^2/sp^3-hybridized carbon atoms) [28]. All of these characteristics make GO and rGO interesting for their own characteristics.

1.5 Motivation and scope of this thesis

Research so far has been directed toward studying as-synthesized GO or toward understanding the reduction process and the effect of reduction chemistry on the sheet properties. As a result, researchers have concentrated on temperatures exceeding ~150°C, so as to be sure of oxygen removal. On the other hand, what happens to GO structures at relatively low temperatures (< 80°C) has been largely unexplored, which is an interesting question to ask knowing that as-synthesized GO is a metastable material and its structure can change even at such mild temperatures. We believe this is an important gap to be filled because:

1. By doing so, we can establish a complete theory for structural evolution of

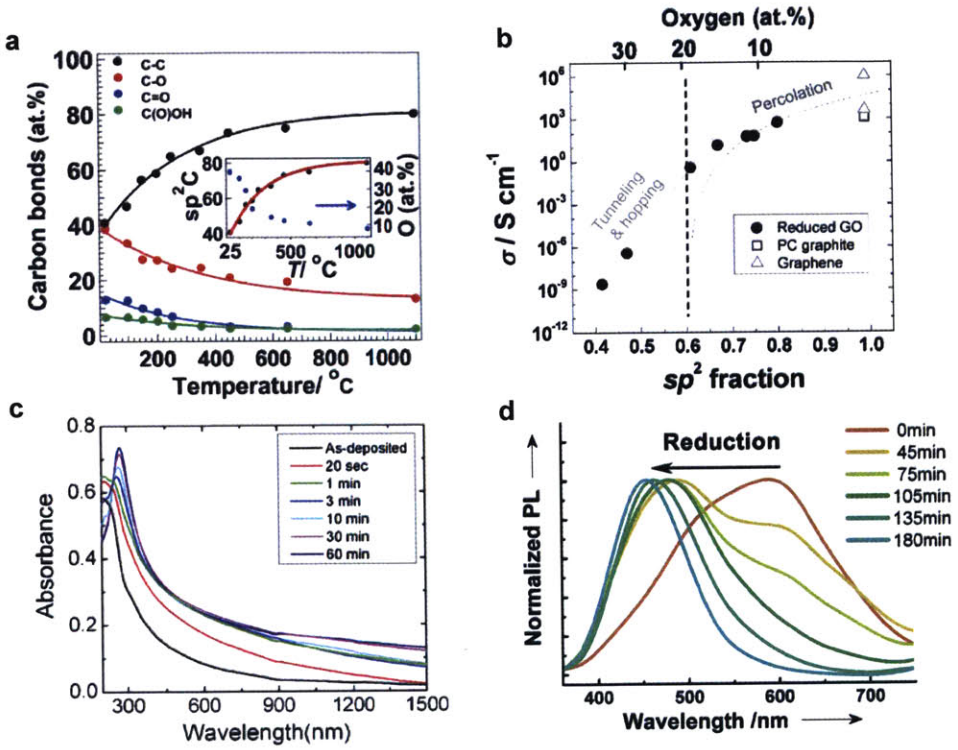

Figure 1.4: Evolution of sheet properties with reduction of GO. (a) Evolution of sp^2 C=C carbon and different oxygen functionalities at different annealing temperatures. The inset correlates the total oxygen concentration with the sp^2 C=C content at different reduction temperatures (taken from Ref. [28]). (b) Conductivity of rGO thin films as a function of the sp^2 C=C content/oxygen content (taken from Ref. [28]). (c) Increasing optical absorption, especially in the visible, upon chemical reduction of GO in hydrazine for various times (taken from Ref. [36]). (d) Evolution of the photoluminescence (PL) spectra revealing a blue shift upon chemical reduction of GO in hydrazine for various times (taken from Ref. [37]).

GO over the entire range of temperatures, i.e. from room temperature to ~1000°C, which is currently lacking.

2. If we find interesting structural transitions, this would enable us to predict and control the sheet properties in new ways, as opposed to reduction, which is to date the only handle to control the structure of GO. This could potentially open the door for completely new applications or for enhancing the performance of existing applications based on GO.

3. Devices that may incorporate GO in the future will most likely be subjected to mild temperatures and knowing what happens then would be critical for smooth functioning of such devices.

The main aim of this thesis is to investigate what happens to GO structures at moderate temperatures (50-80°C) and fill a gap in the theory of structural evolution of GO. Specifically, we have performed a combination of computations and experiments to pinpoint a new structural transition in GO at such temperatures. Further, we have utilized this structural transition for two different applications: 1) Improving the quality of rGO films obtained from GO, and 2) Achieve efficient functionalization of GO with foreign molecules for enhanced biosensing applications.

- Chapter 2 shows how we first understood the structure-property relationships in GO at the atomic-scale by utilizing computer simulations and ab initio computations.

- Chapter 3 reveals how the idea of a new structural transition in GO was developed and validated through experiments, based on the understanding

gained through computer simulations (as described in Chapter 2).

- Chapter 4 shows two possible ways to translate the benefits of structural transition into device-scale applications.
- Chapter 5 summarizes key findings of this thesis and discusses possible future directions.

Chapter 2

Understanding structure-property relationships in GO and rGO through theory and simulation

2.1 Why understand structure-property relations in GO and rGO?

As noted in Chapter 1, one of the notable features of the reduction process of GO is the opportunity gained in tuning the materials electronic and optical properties. This aspect is well documented and is attributed to the tunable fraction of the sp^2/sp^3-hybridized carbon atoms (or the tunable oxygen content). While these are certainly important control knobs, there are untapped opportunities that could lead to further enhancement of the sheet properties.

For instance, a key handle that has the potential to further tune the electronic

and optical properties is the type and fraction of the various functional groups present in GO/rGO. To recap, these functional groups are epoxies, hydroxyls, carbonyls, ethers and carboxyls, in addition to defects such as carbon chains and vacancies that are introduced during the reduction process [8]. Further, GO/rGO structures are metastable in nature [24, 38]. Given time and under the application of a suitable external stimulus, one can potentially alter their structures and drive them into completely new states, which can give rise to interesting sheet properties.

In order to tap into these promising avenues, one needs to understand the structure at the atomic level, and how the individual oxygen functional groups and their covalent interaction with the underlying carbon atoms affect the macroscopic sheet properties. Specifically, our interest lies in understanding the impact of oxygen functional groups on the stability, electronic and optical structure of GO/rGO structures.

2.2 Why are simulations necessary to achieve this task?

Thus far, in experiments, it has been a daunting task to probe the molecular structure and paint an accurate picture of the structure-property relationships, as fabricated GO/rGO structures are highly disordered and chemically inhomogeneous. Instead, atomistic simulations can be employed to achieve an in-depth understanding of the main trends in structure-property relations. For instance, molecular dynamics (MD) simulations of thermal reduction of GO have predicted the formation of stable carbonyl and ether groups in addition to the widely known

epoxy and hydroxyl groups, confirming the nature of rGO as highly disordered and chemically inhomogeneous [39, 8]. Density functional theory (DFT) calculations have previously shown the presence of electronic band gaps in GO/rGO structures [40, 41, 42, 43]. However, these DFT simulations have focused mainly on simple and ordered structures, containing a mixture of epoxy and hydroxyl groups without accounting for the realistic, disordered configurations of GO/rGO. Hence, only limited insights have been obtained so far through simulations.

2.2.1 Computational strategy used in this thesis

In order to address the above issue and to develop a bottom-up design methodology for understanding the realistic amorphous structure of GO/rGO and its impact on the properties, we followed a specific computational strategy.

- Using classical MD simulations based on reactive force fields, we have obtained hundreds of realistic structures of GO and rGO, with different oxygen concentrations and functional group compositions, which agree well with experimental observations [8, 44].

- Ab initio DFT calculations were then employed to compute and understand the stability, electronic and optical properties using the so-generated realistic set of GO/rGO structures.

- Based on this understanding, we were able to predict new mechanisms in metastable GO/rGO structures and in turn control their sheet properties in unique ways, thus opening the door for new applications or enhancing the performance of existing applications based on GO/rGO.

Using a combination of classical MD and DFT simulations is necessary because of the following reasons.

- We are interested in preparing realistic GO/rGO structures. We understand that structural changes upon the application of an external stimulus such as temperature, take place on the order of seconds to minutes. Further, we need to account for the amorphous nature of GO/rGO, which requires using a big set of sufficiently large structures. Also, the conversion of GO to rGO involves breaking of existing bonds and formation of new bonds. In order to account for these important issues, we chose to prepare structures using classical MD simulations with reactive force fields. Although MD simulations are limited to ps-ns timescales, by increasing the temperature of the system, one can drive the kinetics upwards and realistic structures can be obtained. ReaxFF, a type of reactive force field developed by the Van Duin group is chosen for our simulations, since it is known to accurately describe bond-breaking and formation events in hydrocarbon systems [44].

- Subsequently, we are interested in understanding the impact of the realistic structure on the electronic structure of the material, which requires one to employ ab initio calculations. DFT strikes that balance between accuracy and computational efficiency, has been shown to be accurate for these material systems [39, 40]. Importantly, it is known to accurately predict the properties that we are interested in, i.e. the stability (total energy) and electronic band structure. Hence, we chose to use DFT methods.

2.3 Correlating atomic structure with sheet properties of rGO

The first direction we took in this thesis was toward understanding how the different atomic features in rGO structures affect their sheet properties. Specifically, we wanted to understand the impact of different functional groups on the stability, work function and photoluminescence (PL) characteristics of rGO. This is because understanding and tailoring the work function of rGO has not been addressed thus far, although one of the current thrusts in rGO research is towards designing large-scale ultra-thin transparent conducting electrodes for applications such as transistors, batteries and solar cells [14]. Further, rGO is a promising material for low-cost, solution-processable optoelectronic devices owing to its tunable PL spectra (blue to red regions) [36, 37].

2.3.1 Structures adopted for computational synthesis

Figure 2.1a shows our preparation protocol of rGO structures. The functional groups on the basal plane of GO are known to mainly consist of epoxy and hydroxyl groups, with the presence of five- and six-membered-ring lactols, carboxyl groups along the periphery of the sheets. We create periodic GO sheets with randomly distributed epoxy and hydroxyl groups on both the sides of the graphene plane in accordance with the known presence of these groups in GO sheets [23, 8, 6]. Since GO is non-stoichiometric and kinetic factors lead to local variations in the oxygen concentration, we use different oxygen concentrations of 15%, 20% and 25% (by mixing in the form of epoxy and hydroxyl groups) to construct GO sheets [8].

We employ epoxy to hydroxyl ratios of 3:2, 1:1 and 2:3 to account for composition fluctuations during the synthesis of GO. Next, using MD simulations, we performed high temperature reduction of GO structures at 1500 K in vacuum to generate rGO sheets with oxygen concentration in the 10-20% range, as widely encountered in the experiments. All rGO structures were then relaxed within DFT for structural optimization before computing sheet properties of interest (see appendix for more details on computational methods).

2.3.2 Sheet morphology

Our thermal reduction simulations lead to the formation of disordered rGO structures with a range of functional groups, such as epoxy and hydroxyl groups initially present in rGO, carbonyl and ether groups, three- and five-membered carbon rings, quinones, and carbon chains (Figure 2.1b and 1.3b), consistent with previous computational work [8]. The generation of a large number of structures allows us to establish statistically meaningful averages for the relative distribution of functional groups present in rGO after the reduction process. Figure 2.1c shows a key trend we observe in our simulations, namely that thermal reduction of epoxy-rich GO (initial epoxy to hydroxyl ratio of 3:2) results in carbonyl-rich rGO structures, whereas thermal reduction of hydroxyl-rich GO (initial epoxy to hydroxyl ratio of 2:3) results in hydroxyl-rich rGO structures.

2.3.3 Stability of rGO structures

We employ DFT calculations to study their kinetic stability. As discussed above, structural and chemical modifications of as-prepared rGO can result in undesirable

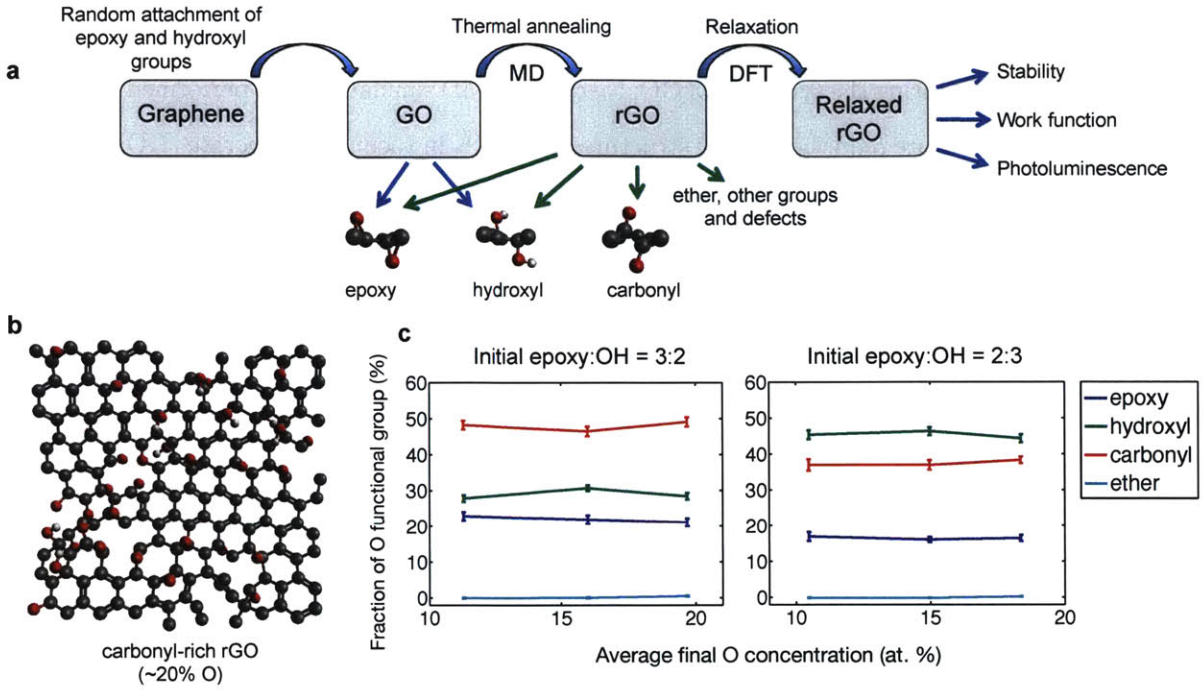

Figure 2.1: Morphology of generated rGO structures. (a) Schematic of the preparation protocol of rGO. (b) Representative disordered carbonyl-rich rGO structure. Carbon, oxygen and hydrogen are represented as black, red and grey spheres, respectively. (c) Average fraction of oxygen-containing functional groups as a function of average final oxygen concentration in the rGO sheets, for different initial GO structures with epoxy to hydroxyl ratios of 3:2 (left) and 2:3 (right). The thermal reduction of these two cases results in, respectively, carbonyl-rich rGO (left) and hydroxyl-rich rGO (right). In each plot, the results are obtained by averaging over 40 rGO structures, and the error shown represents the standard error of the mean calculated for the same set of structures.

changes in functionality limiting its applicability in optoelectronic devices. We compare the relative stability of rGO structures by computing the formation energy of carbonyl-rich and hydroxyl-rich rGO structures as a function of oxygen and hydrogen chemical potentials (or equivalently, partial pressures) as shown in 2.2a.

The formation energy is calculated as:

$$E_{form} = E_{tot}(C_l O_m H_n) - lE(C_{gr}) - m\mu_O - n\mu_H$$

where $E_{tot}(C_l O_m H_n)$ is the total energy of the rGO structure with l carbon, m oxygen and n hydrogen atoms, $E(C_{gr})$ is the energy of a carbon atom in a pristine graphene sheet [43], and the reference chemical potentials of oxygen (μ_O) and hydrogen (μ_H) are chosen as those of the oxygen and hydrogen in O_2 and H_2 gas molecules, respectively [43, 45].

The computed trends seen in the formation energies of carbonyl-rich and hydroxyl-rich rGO structures suggest that hydroxyl-rich rGO with low oxygen content is favorable over a wide range of oxygen partial pressures. Conversely, the formation of carbonyl-rich structures (with higher oxygen content) are preferred only at high oxygen partial pressures. On this basis, we suggest that while as-synthesized rGO commonly possesses large fractions of oxygen-rich epoxy and carbonyl groups, [46, 8, 47] these structures are only kinetically stable. When exposed to milder conditions of temperature and O_2 or H_2 gas partial pressures than those used during the reduction process, such structures evolve through a variety of spontaneous reduction mechanisms towards hydroxyl-rich rGO structures with lower oxygen content. This prediction appears to be corroborated by recent experimental work from Kim *et al.*, [38] where as-synthesized multilayer GO films rich in epoxy groups showed a similar metastability and evolved towards hydroxyl-rich GO at room temperature. A key mechanism involved in this spontaneous reduction of rGO is water formation via the interaction of hydrogen and oxygen atoms within the basal plane, a process observed to be favorable at room temperature

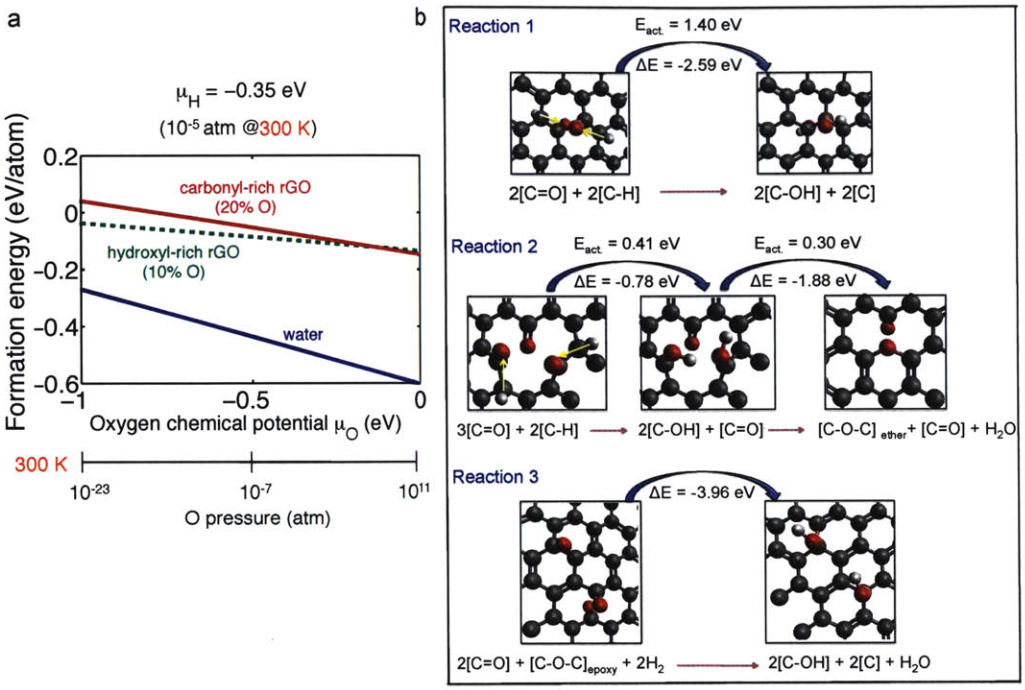

Figure 2.2: Stability of as-prepared rGO structures. (**a**) Formation energy per atom of hydroxyl-rich (10% O) and carbonyl-rich (20% O) rGO structures as a function of oxygen chemical potential, shown for the standard value (-0.35 eV) of atmospheric hydrogen chemical potential at 300 K. The energetics shown in the plot indicates the higher stability of hydroxyl-rich rGO compared to carbonyl-rich rGO, and the tendency of both to undergo a reduction process *via* elimination of water. (**b**) The three reaction mechanisms studied here for the conversion of carbonyl groups to hydroxyl groups in the presence of chemisorbed H atoms. Reactions 2 and 3 involve reduction *via* elimination of water, while reaction 1 does not involve water formation.

and under ambient atmospheric hydrogen and oxygen partial pressures (see Figure 2.2a).

In order to elucidate the atomistic mechanisms involved in the reduction of carbonyl-rich to hydroxyl-rich rGO, we examined three possible reaction pathways (Figure 2.2b) capable of converting carbonyl to hydroxyl groups in rGO, and

quantified the associated energetics using nudged elastic band calculations. Since carbonyl groups occur commonly in pairs or at the periphery of carbon vacancies in rGO, we consider two reaction schemes involving a carbonyl pair or a carbonyl-vacancy pair (respectively, Reaction 1 and 2 in 2.2b). In addition, we investigate a third reaction scheme (Reaction 3 in Figure 2.2b) where the interaction of a carbonyl group with an epoxy group leads to rGO reduction, a case chosen to emphasize the importance of interplay between functional groups in the rGO sheet. In our proposed reaction schemes, hydrogen is assumed to be present in chemisorbed form (within C-H bonds), as commonly generated during GO synthesis [38] or exposure to air. As a result, the three proposed reaction mechanisms are limited by the diffusion of C−H bonds across the basal plane (a process known to have an energy barrier of 0.55 eV [38]) and by the availability of H in the environment.
In the first reduction mechanism (Reaction 1 in Figure 2.2b), a carbonyl pair interacts with chemisorbed H and forms a hydroxyl pair, with an energy gain obtained from our DFT calculations of 2.59 eV. The second reduction mechanism (Reaction 2 in Figure 2.2b) is a two-step process: in the first step, carbonyl groups at the periphery of a carbon vacancy react with hydrogen to form hydroxyl groups, with a calculated energy gain of 0.78 eV. In the second step, the interaction between the so-formed hydroxyl groups leads to water formation and elimination of the vacancy by forming an ether group, a process with an energy gain of 1.88 eV based on our calculations. In the last reaction scheme proposed here (Reaction 3 in Figure 2.2b), a carbonyl pair and an epoxy group interact to form two hydroxyl groups and a water molecule with a predicted energy gain of 3.96 eV. Our calculations suggest that all mechanisms considered here are energetically favorable, and are thus predicted to occur thermodynamically; the computed energetics confirms

the tendency of rGO to undergo further reduction and "self-heal" over time by restoring sp^2 carbon atoms in the graphene lattice.

We estimate the kinetics of Reactions $1-3$ by computing their rates using the Arrhenius formula:

$$k = k_0 \exp(-E_{act}/kT)$$

where E_{act} is the activation energy computed using the nudged elastic band method (Figure 2.2b), and k_0 is an attempt frequency with an assumed commonly used value of 10^{13} hz. NEB is a method for finding saddle points and minimum energy paths between known reactants and products. The method works by optimizing a number of intermediate images along the reaction path [48]. At room temperature (300 K), we predict Reactions 1 and 3 to possess a high activation energy of 1.40 eV limited by the process of 'hole' closure in these cases, causing a slow reaction rate of $k \approx 10^{-11}$ hz. For comparison, the first step of Reaction 2 involving a chemical process similar to Reaction 1 (in terms of converting carbonyl to hydroxyl groups) but occurring near C vacancies is significantly faster, achieving an estimated carbonyl-to-hydroxyl conversion rate of 10^6 hz, and involving a significantly lower energy barrier of 0.41 eV. Our calculations suggest that the higher activation barrier for Reaction 1 is related to the presence of strain during the carbonyl pair reaction, while in Reaction 2 strain is reduced due to the presence of a vacancy in the basal plane. The increased reduction rate found here near C vacancies is consistent with the recent experimental observation of spontaneous healing of nano-holes in graphene.[49] On the basis of the combined thermodynamics and kinetics of the processes considered here, we conclude that although rGO obtained *via* thermal annealing is kinetically stable with a significant fraction of

carbonyl groups [8], our findings indicate the metastability of these structures and their structural evolution towards hydroxyl-rich rGO over time. The sensitivity of the optical and electronic properties on functional group composition discussed below makes it clear that the controlled application of rGO in existing technologies cannot ignore such important stability considerations and chemical transformation processes.

2.3.4 Work function of rGO structures

In what follows, we perform DFT calculations on the library of realistic rGO structures generated in this work, with the goal of studying the dependence of the work function and electronic structure of rGO on the concentration of different functional groups. In particular, we explore the impact of two crucial parameters on the work function: 1) the overall oxygen concentration, and 2) the concentration of different types of functional groups. The work function tunability in rGO structures stems from the formation of dipoles between carbon and oxygen atoms with different electronegativity. In rGO, oxygen atoms in carbonyl, epoxy, and hydroxyl groups are located outside the graphene basal plane, and form C−O bonds of different types and with different chemical surroundings. As a consequence, the strength of the dipole moment in rGO can be tuned by varying both the overall oxygen content and the concentration of different functional groups.

In Figure 2.3a, we show the results of our DFT calculations for rGO structures prepared with our reduction protocol and resulting in oxygen concentrations in the $10 - 20\%$ range. Within this oxygen concentration range, the work function is found to be tunable between $5.0 - 5.5$ eV, thus allowing a 0.5 eV variation

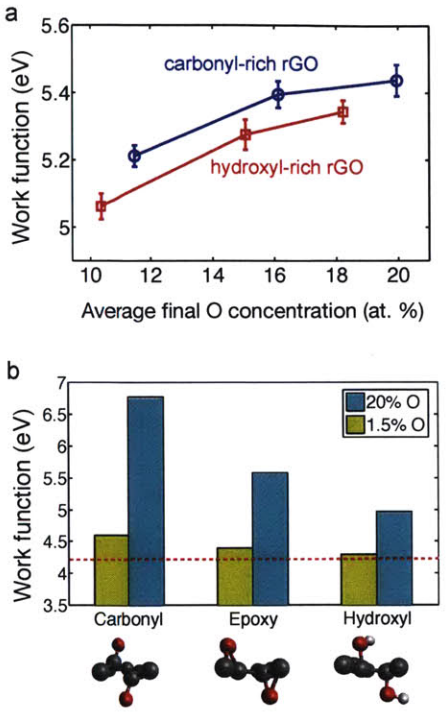

Figure 2.3: Work function tunability in rGO structures. (**a**) Calculated work function of carbonyl-rich and hydroxyl-rich rGO structures with different oxygen content. (**b**) The effect of individual functional groups on the work function of rGO, for two different total oxygen concentrations of 1.5% (for validation purpose) and of 20%. Carbonyl groups show the largest impact on the work function among all groups, inducing a work function value 60% higher than that of graphene (4.2 eV, shown here for reference as a dashed red line).

within this range by adjusting the reduction conditions. We expect the tunability to increase further if a wider oxygen concentration range is considered.

Despite this favorable effect, we demonstrate here that oxygen concentration is not the main variable controlling the work function, and that a significantly higher work function tunability (up to 2.5 eV) can be obtained by varying the fraction of a single type of functional group. In order to isolate the impact of

different functional groups on the work function, we carried out DFT calculations on smaller structures (approximately 130 atoms) than considered above, containing only one type of functional group – epoxy groups, hydroxyl groups, and carbonyl groups. In each case, we consider two values of the total oxygen concentration: 20%, considered here as an upper limit of oxygen concentration in rGO, and 1.5% used here to validate our method by assuring that in the limit of a graphene structure with only one oxygen-containing functional group a work function value close to that of pristine graphene (4.2 eV) is obtained. For intermediate oxygen concentrations, the work function varies continuously within the range delimited by these two cases.

Figure 2.3b shows our calculated work function for structures with a single type of functional group. We observe the dominant effect of carbonyl groups, as seen by work function values in the $4.4 - 6.8$ eV range for rGO structures containing only carbonyl groups. This represents a 60% increase compared to the computed work function of graphene (4.2 eV), an effect we attribute to the large dipole moment of the C–O double bond in carbonyl groups. We find a considerable impact on the work function also in the case of epoxy groups, yielding work function values in the $4.35 - 5.6$ eV range, representing an increase by up to 32% compared to graphene. For hydroxyl groups, we observe a more moderate effect, yielding work function values in the $4.25 - 4.95$ eV range, up to 17% higher than graphene. It's worth noting that in all cases considered, the work function is never lower than that of graphene, due to the orientation of the C–O dipoles pointing outward from the basal graphene plane in all cases considered. Our results explain recent experimental work showing a wide range of work function values in rGO [50, 51, 20], which we interpret as a consequence of different content of

functional groups resulting from different experimental reduction protocols used.

We conclude that in order to take full advantage of the wide range of achievable work functions in rGO, experimental reduction techniques yielding rGO with specific types of functional groups should be devised. Recently suggested routes towards synthesis with functional-group control include using hydrogen to adjust the proportion of carbonyl and hydroxyl groups, [8] dissociating oxygen molecules in ultra-high vacuum to achieve selective epoxy functionalization, [24] or the use of local reduction methods with nanometer resolution [52].

2.3.5 PL spectra of rGO structures

Similar to the work function, the PL emission spectrum of rGO shows significant tunability when the oxygen concentration and the ratios of different functional groups are varied [36, 37]. PL spectra of rGO samples commonly show two prominent features: a broad emission peak centered around $500 - 600$ nm ($2 - 2.5$ eV photon energy, denoted as I_{P1}) and a narrow peak centered around $450 - 475$ nm ($2.6 - 2.75$ eV photon energy, denoted as I_{P2}) [37]. The energy of the narrow I_{P2} peak is known to depend on the size of sp^2-hybridized graphene domains within the rGO matrix [37]. The broad I_{P1} peak, on the other hand, is thought to be determined by disorder-induced defect states. However, a clear understanding of the effect of different functional groups present in rGO is still missing, and structural models employed so far to account for the nature of the I_{P1} peak can only provide a qualitative picture of the role of disorder [36, 41, 37].

We perform here DFT electronic structure calculations on selected samples within our database of rGO structures, with the objective of elucidating the nature

of the PL peaks in rGO at the atomistic level, and to decompose the contributions of different functional groups to the I_{P1} PL emission peak. Figure 2.4a shows the electronic structure of two carbonyl-rich rGO samples with respectively low (10%) and high (20%) total oxygen concentration, expressed as the projected density of states (PDOS) from carbon atoms in the rGO structure. The carbon PDOS is chosen here as the main variable since in rGO the frequency and intensity of peak PL emission are governed by the π and π^* "tail" electronic bands, arising from carbon p_z states.

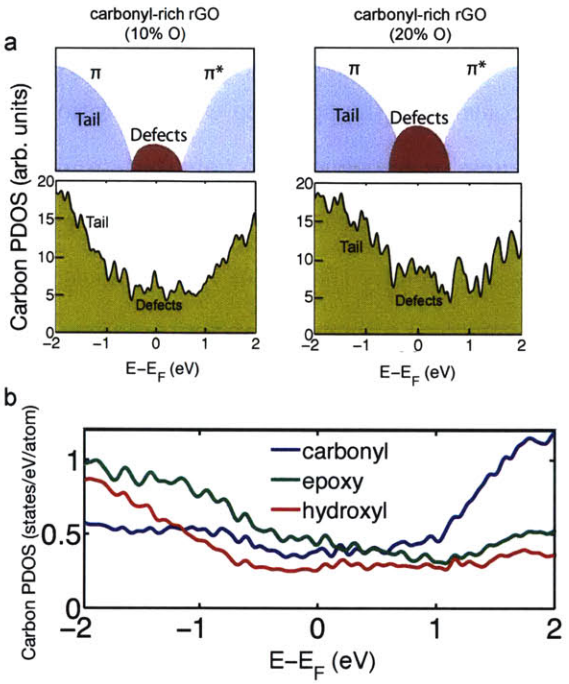

Figure 2.4: Photoluminescence in rGO structures. (**a**) Carbon PDOS plots for carbonyl-rich rGO with 10% (left) and 20% (right) oxygen concentrations. Above the plots, the contribution of defect and $\pi-\pi^*$ tail states to the PDOS is shown schematically for the two cases. (**b**) PDOS from carbon atoms in carbonyl, epoxy and hydroxyl groups.

Figure 2.4a shows the presence of a significantly higher fraction of defect states

around the Fermi energy (E_F) for the rGO sample with higher oxygen concentration, with the formation of a well defined PDOS feature between the π and π^* tail bands. We decouple the contribution of individual functional groups to the tail and defect states by computing the average PDOS arising from carbon atoms attached to different functional groups (2.4b). Our analysis shows that the valence band (π tail) states are localized mainly at epoxy groups, while the conduction band (π^* tail) states are mostly contributed by carbonyl groups. On this basis, we suggest that it may be possible to control the π and π^* tail bands by varying the ratio of epoxy and carbonyl groups. Assuming that the peak PL emission energy is set by the energy difference between the peaks in the DOS of the π and π^* tail bands, a similar strategy of controlling the epoxy to carbonyl ratio could also allow one to tune the peak PL emission frequency. We note that an increase in the fraction of epoxy and carbonyl groups at the expenses of hydroxyl groups causes a higher density of defect states, as seen by the higher PDOS values around E_F for epoxy and carbonyl groups compared to hydroxyl groups in Figure 2.4b. The possibility outlined here to combine distinct contributions from different functional groups to the PL is a unique feature of rGO, and will be the object of further investigation.

2.4 Appendix

2.4.1 Computational details

MD simulations used to prepare the rGO structures were carried out using the LAMMPS package [53] with the ReaxFF reactive force-field, chosen here for its ability to accurately describe bond-breaking and formation events in hydrocarbon

systems. [44] We employed a time step of 0.25 fs and the NVT Berendsen thermostat. [8] Initial GO structures consisted of a 2.2 x 2.1 nm periodic graphene sheet containing 180 C atoms with randomly distributed epoxy and hydroxyl groups on both sides of the sheet [39]. During the reduction process, the temperature of the GO sheets was increased from 10 K to 1500 K over a time interval of 250 fs. The system was then annealed at 1500 K for 250 ps to allow for structural stabilization. Molecular by-products released from the GO sheet were removed and the system was further annealed at 300 K for an additional 1.25 ps to confirm its stability.

rGO structures generated with this approach were further relaxed (to less than 0.03 eV/Å residual atomic forces) using DFT with a plane-wave basis set as implemented in the VASP package. [54, 55] In all the DFT calculations presented in this work, we used the Projector Augmented Wave (PAW) method to describe the core electrons [56] and the Perdew-Burke-Ernzerhof exchange-correlation (XC) functional [57] in combination with a gamma-point $\vec{k}$-grid. The wave function and charge density were expanded in plane waves with a wavefunction kinetic energy cut-off of 500 eV. A vacuum region of 16 Å was used in the direction normal to the sheets. For the study of reaction paths and energy barriers used to determine the kinetic stability of rGO, we employed nudged elastic band (NEB) calculations as implemented in VASP with $9 - 13$ image structures between the reactant and the product.

Chapter 3

A new phase transformation in GO: Clustering of oxygen atoms under mild thermal annealing

3.1 Ideation of a new structural transition in GO

Chapter 2 demonstrates the advantages of using accurate atomistic calculations to not only predict realistic nanoscale structures, but also to understand how the atomic features influence the macroscale sheet properties. One important observation we made in our simulations was the metastable nature of rGO structures, especially at higher oxygen concentrations. This led us to think that as-synthesized GO, which has high oxygen concentration, could be relatively more unstable and hence show a greater propensity to evolve into thermodynamically more stable structures, even under the application of a weak external stimulus.

In literature, metastability of GO structures has been highlighted on numer-

ous occasions [24, 38]. However, structural transitions - other than reduction - have been largely unexplored. It is well known that for temperatures larger than 120-150°C and with greater annealing time, oxygen removal occurs leading to the formation of rGO. The boundary demarcates the two phases GO and rGO. However, what happens to GO structures at relatively mild annealing temperatures (50-80°C) has been largely unexplored. An important question arises: *Does the structure of GO remain largely unperturbed under these conditions, or can we expect a structural change in GO without changing its oxygen content, thereby leading to new forms of GO?*

It is generally well accepted that oxygen atoms are randomly distributed on the graphene basal plane. We asked the following question - *Would the stability of GO phases change - at a fixed oxygen concentration - if the oxygen atoms formed clusters, instead of being randomly distributed?* (see Figure 3.1). In other words, does the stability of mixed sp^2-sp^3 GO phases change when they separate into distinct sp^2 (graphitic) and sp^3 (oxidized) domains [58].

3.2 Simulations to predict the energetics of structural transition

3.2.1 Thermodynamics

In order to answer the above question, we carried out a stability analysis of GO structures using a combination of classical MD simulations based on reactive force fields [44], and DFT calculations. Model GO structures with different sizes of oxidized and graphitic domains (none, three and six graphene rows) were prepared

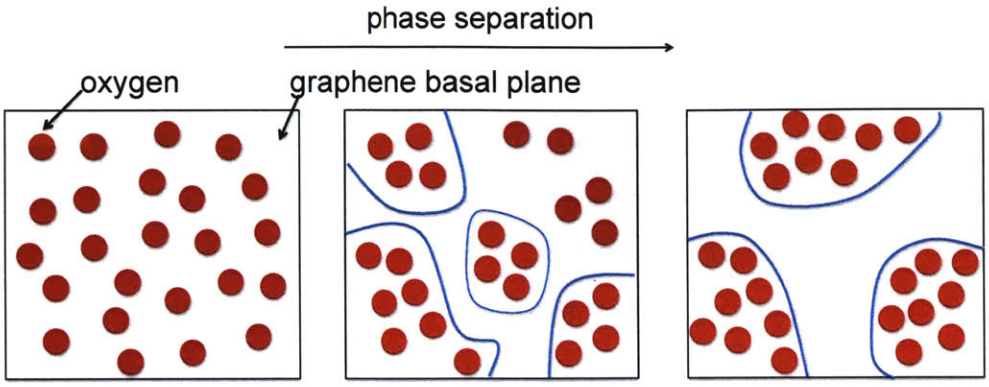

Figure 3.1: Phase transformation of GO structures. Schematic depicting the phase-separation process in as-synthesized GO structures from a mixed sp^2sp^3 phase into two distinct oxidized and graphene phases through diffusion of oxygen atoms on the graphene basal plane under the influence of an external stimulus.

with the oxygen concentration kept fixed to mimic the phase-separation process (Figure 3.2a). Initially, the oxidized domains consisted of randomly distributed epoxy and hydroxyl groups attached to both sides of the graphene sheet, consistent with previous work that shows the dominant presence of such functional groups in GO [23, 8, 6]. To account for local variations in oxygen concentration and the fraction of functional groups on the GO sheet, we studied oxygen concentrations of 10 and 20% in the initial GO structures and prepared samples with epoxy to hydroxyl ratios of 3:2 and 2:3 [8]. GO structures were then annealed at 300 K using MD simulations, using the procedure described in Chapter 2.

Our MD simulations produced GO structures that consisted of bare graphitic domains in conjunction with oxidized domains that largely contained epoxy and hydroxyl functional groups with a small amount of carbonyls and water molecules, consistent with previous computational work [38]. The generation of ten samples for each composition allows us to present meaningful averages of the computed

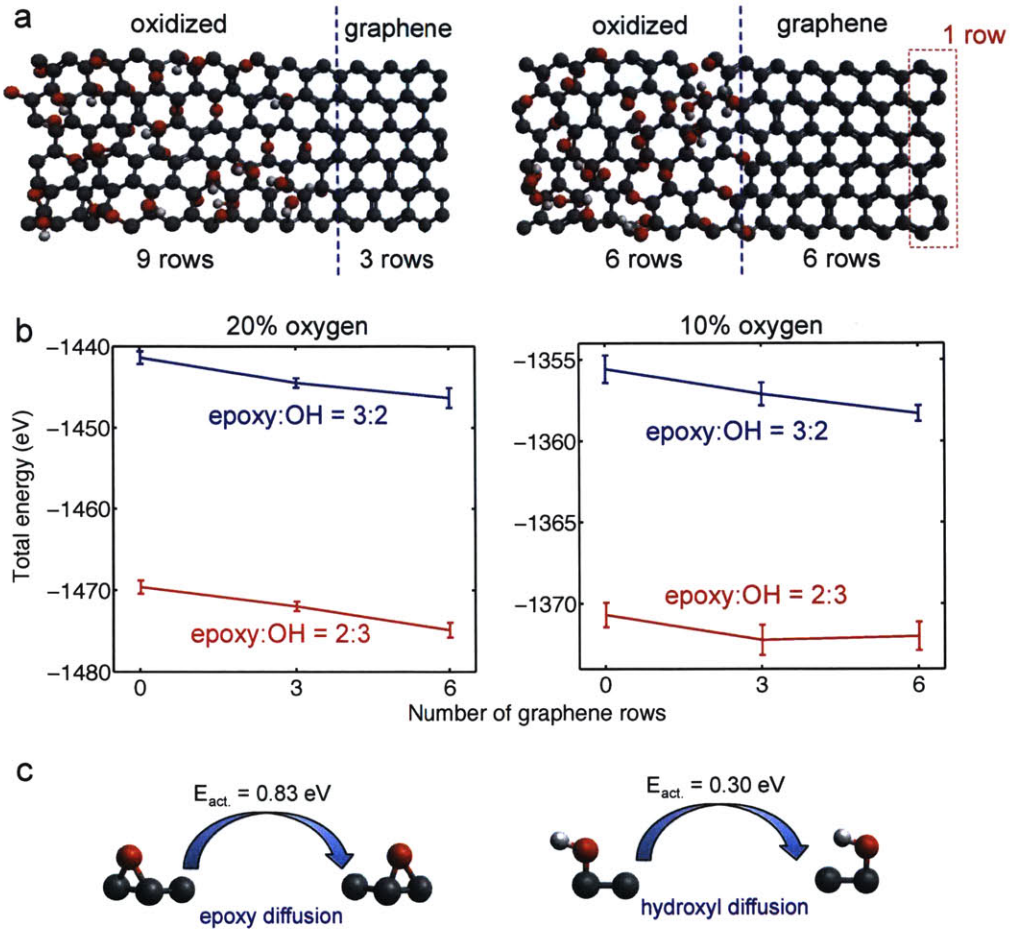

Figure 3.2: Phase separation in GO structures (a) Representative model GO structures used to compute the energetics of the phase separation process. Each structure consists of two distinct oxidized and graphene phases with different domain sizes. Carbon, oxygen and hydrogen are represented as grey, red and white spheres, respectively. (b) Formation energy values of phase separated GO structures as a function of the graphene domain size for different oxygen contents and epoxy to hydroxyl functional group ratios. The formation energies decrease upon phase separation indicating the process to be thermodynamically favorable. In each plot, the results are obtained by averaging over 10 GO structures for each data point, and the error bars shown represent the standard error of the mean calculated for the same set of structures.

properties. Figure 3.2b shows the total energy of the phase-separated GO structures computed from our MD simulations (internal energies at 300 K). We observe that the total energies decrease with increasing phase separation, that is, with increasing graphitic domain size, which suggests that the process of phase separation is thermodynamically favorable in GO structures. Additional calculations, performed using chemically homogeneous and ordered phases of GO, indicate similar trends and favorability of the phase-separation process. We attribute this favorability to strain compensation and hence strain relief in the GO structures. For instance, although two isolated oxygen groups attached on either side of the graphene sheet increase strains in their vicinity, the same oxygen groups can partially cancel these strains when present in proximity to one another, and thus favor phase separation and clustering of oxygen atoms on graphene [43, 59, 60, 61].

3.2.2 Kinetics

A key mechanism involved in the phase-separation process during annealing is the diffusion of epoxy and hydroxyl functional groups along the graphene basal plane. Our calculations show that diffusion of an isolated epoxy group is limited by an activation barrier of 0.83 eV, and the barrier for diffusion of an isolated hydroxyl group is 0.30 eV, much lower than that in the epoxy case (see Figure 3.2c). Although diffusion of oxygen atoms at room temperature has been observed in GO multilayers previously, the structural changes were discernible only after months, which implies extremely low diffusion rates [38]. Using the Arrhenius formula $k = k_0 \exp(-E_{act}/kT)$, where E_{act} is the computed activation barrier and k_0 is the attempt frequency (assumed to be constant), we estimate the hydroxyl

and epoxy diffusion to increase by one and two orders of magnitude, respectively, at 80°C (353 K) compared with their diffusion at room temperature (300 K).

These calculations suggest that the structural changes due to oxygen group diffusion can be triggered using mild annealing temperature (50-80°C) as an external stimulus. Further, our calculations suggest that these changes can be observed at relatively smaller time scales (days) at these temperatures, in contrast to months reported for stock solutions preserved at room temperature [38]. However, caution needs to be exercised in not treating the GO samples at higher temperatures (> 150°C), since the process of oxygen removal becomes activated and competes with the oxygen diffusion process.

3.3 Experimental realization of the structural transition

3.3.1 Sample preparation

In order to realize the phase transformation of GO sheets in experiments, GO sheets were first synthesized by the Hummers' method [26]. We performed thermal annealing studies on GO suspensions, freeze-dried GO (fd-GO) samples and GO thin-film samples. GO suspensions were prepared by thoroughly exfoliating GO sheets in water. Once these suspensions were obtained, stock solutions were freeze dried to obtain dry, foamy fd-GO samples. Two types of thin-film GO samples were prepared: 1) GO solutions were also drop-cast onto clean silicon substrates and allowed to dry overnight, and 2) GO suspensions were subjected to vacuum filtration onto cellulose substrates, dried overnight and lifted off from the cellulose

substrate to obtain freestanding GO thin films.

GO samples were annealed at 50 and 80°C in a temperature-controlled oven. We chose to perform annealing at two different temperatures so as to understand the impact of kinetics on the resulting phase-transformation processes. At each temperature, samples were retrieved at regular intervals of one, three, five, seven and nine days, and stored in a vacuum desiccator at room temperature for further characterization (see Appendix at the end of this chapter for more details on sample preparation and characterization).

3.3.2 Structural evolution under mild thermal annealing

In what follows, we present the results of our studies performed on solid-state samples (thin-films deposited on Si substrate/fd-GO samples), where the effects of the solvent are discounted.

Figure 3.3 shows the variation of the oxygen concentration, sheet resistance and sp^2 C=C-C carbon fraction of the GO thin film samples with annealing time (annealing temperature is 80°C). The oxygen content and the sp^2 fraction are obtained from X-ray photoelectron spectroscopy (XPS) measurements, while the sheet resistance is measured using a four-point probe set-up. It can be seen that the oxygen concentration remains ~33-34% for films throughout the annealing time. In contrast to the oxygen content, the sheet resistance and the sp^2 fraction show a gradual decrease and increase, respectively, over the period of annealing. These results indicate that while the total oxygen content of GO sheets is preserved, the sheet resistance and the sp^2 fraction vary gradually, indicating a reorganization of the oxygen functional groups on the graphene basal plane.

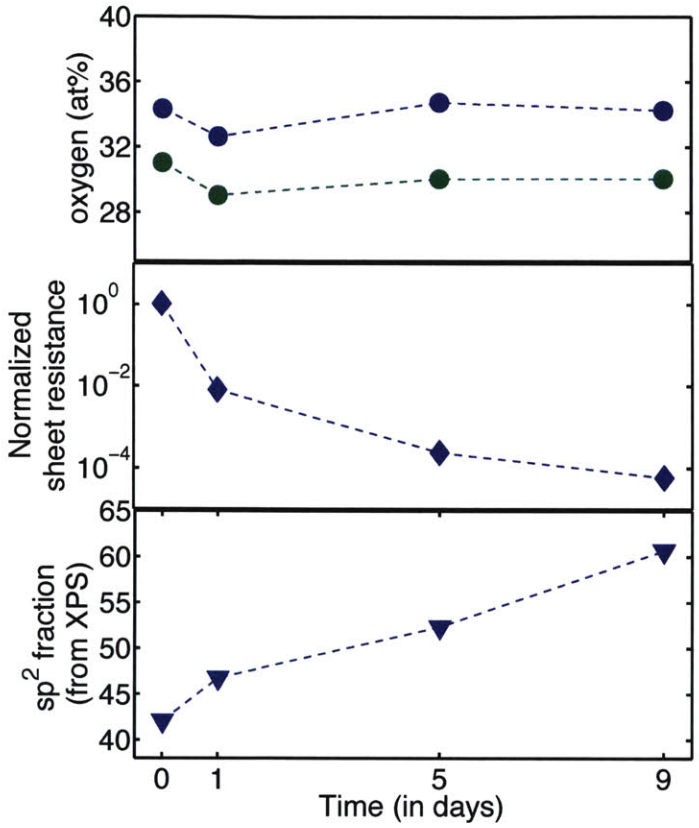

Figure 3.3: Structural evolution of GO structures under mild thermal annealing. Variation of the oxygen concentration, sheet resistance and the sp^2 fraction of GO sheets with mild annealing at 80°C. The oxygen content remains constant, while the sheet resistance and the sp^2 fraction change gradually.

In addition to XPS measurements, we used thermogravimetric analysis (TGA) to monitor the level of reduction of our GO samples during the 80°C annealing run (Figure 3.4a). Although the annealed sample showed an expected slight weight loss (~10%) over the entire course of annealing, attributed to the elimination of physisorbed and interlamellar water [33], the thermogram of a typical as-synthesized GO sample shows an additional significant weight loss (~32%) at an onset temperature of 150°C, attributed to loss of covalently bonded oxygen from the GO sheets. This result shows that our GO samples are not reduced during the entire course of thermal annealing, an observation additionally supporting our XPS measurements and also in agreement with previous reports at these temperatures [33, 62].

We further carried out Fourier transform infrared (FTIR) spectroscopy measurements of GO samples during the annealing process (Figure 3.4b). Importantly, the recorded FTIR spectra clearly show the presence of oxygen functional groups for the entire course of annealing, which again confirms no major removal of oxygen groups from the graphene basal plane. In the case of samples prepared from GO suspensions annealed at 50°C, the absorption peak at 1,620 cm^{-1}, assigned to the C=C skeletal vibrations of graphitic domains or the deformation vibration of intercalated water (scissor mode), remains more or less unchanged for the day 1 case. This peak intensity, however, decreases for the day 5 case, indicating a loss of intercalated water consistent with our TGA results, and a new peak appears with increasing intensity at 1,580 cm^{-1}, attributed to the formation of prominent graphitic domains in GO [33, 62, 63], consistent with the increasing sp^2 fraction measured form our XPS spectra. Our FTIR measurements for the 80°C samples produced similar results where the sp^2 peak appears at day 1, reflecting faster kinetics of the structural transition at this temperature.

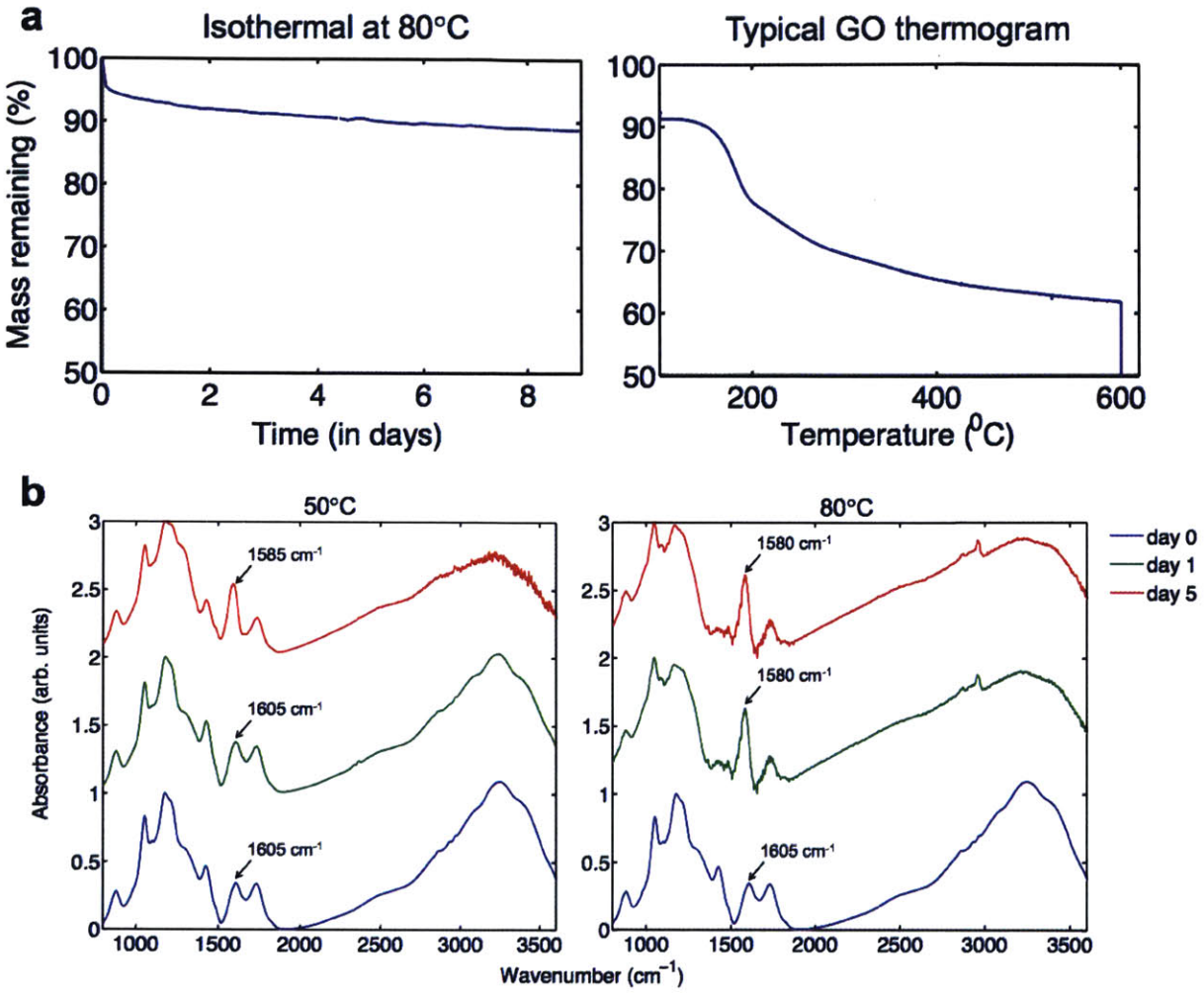

Figure 3.4: TGA and FTIR of annealed GO structures. (a) Recorded mass loss of a GO sample annealed at 80°C for nine days shows only a slight reduction in mass (~10%) compared with a typical TGA thermogram of GO that shows an additional significant mass loss of ~32% because of the removal of oxygen from the basal plane. This indicates that GO is not reduced during the entire course of thermal annealing. (b) FTIR spectra of the GO structures reveal increasing absorption intensities near 1,580 cm-1 attributed to C=C bonds in the case of thermal annealing at 50 and 80°C. This correlates with the increasing sp^2 fraction from XPS spectra and decreasing sheet resistance, which suggests the formation of prominent graphitic domains within the sp^3 matrix.

In order to further corroborate our hypothesis on clustering and prominent formation of sp^2 domains during thermal annealing, we performed Raman analysis on GO thin-film samples. Raman spectra were recorded at room temperature on as-synthesized GO films as well as annealed GO thin-films deposited on a Si substrate. The two prominent features obtained from GO samples (D and G peaks, as shown in Figure 3.5a) were used to analyze our hypothesis of phase separation in annealed GO samples. In a seminal paper by Ferrari and Robertson [64], it is reported that in amorphous carbons, the development of a D peak indicates ordering and clustering of sp^2 domains, exactly opposite to the case of graphite. This trend is observed in the high-defect regime in an amorphous carbon structure. Considering that GO is a 2D amorphous carbon nanomaterial, indeed, our Raman mapping shows an increasing I_D/I_G ratio upon annealing GO thin films at 80°C (Figure 3.5b), indicating ordering and prominent formation of graphitic domains upon thermal annealing [65, 66].

As a means to probe directly the structural transformations taking place in GO, we performed Auger electron spectroscopy (AES) on as-synthesized and annealed GO thin films. The presence of carbon and oxygen on the surface was detected using this technique (Figure 3.6a). Figure 3.6b compares the elemental composition maps (oxygen-rich regions indicated by white spots) of as-synthesized and annealed GO thin films. Clearly, the as-synthesized GO film shows a uniform oxygen composition, and the annealed film shows sharper and segregated regions of oxygen. These results further establish the process of oxygen clustering and development of well-defined graphene-rich domains on annealing as-synthesized GO.

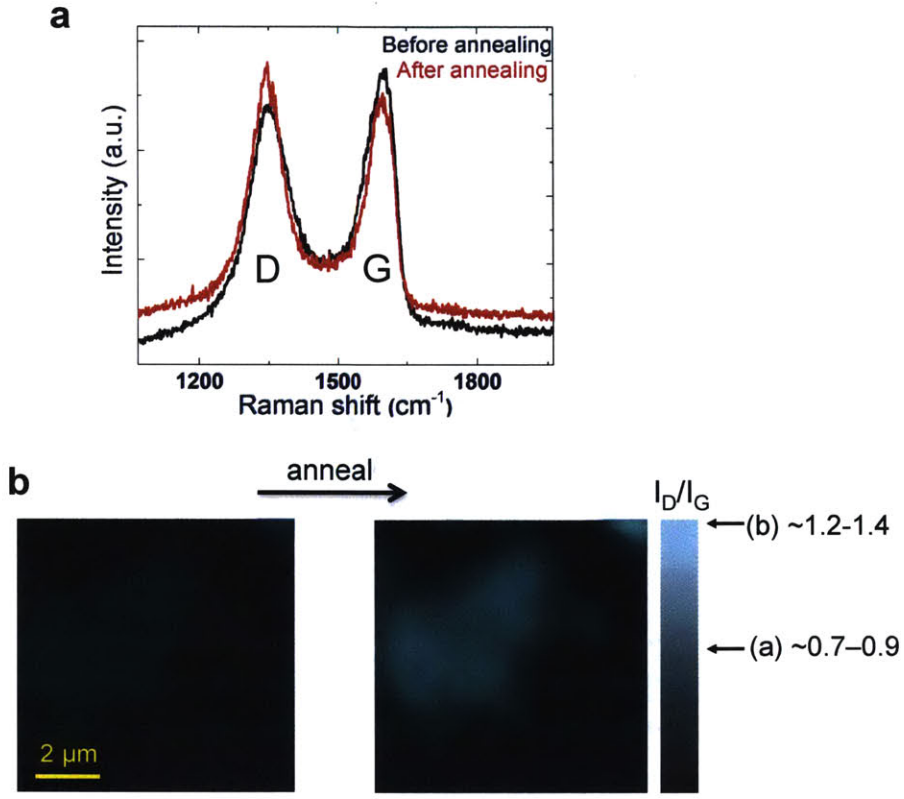

Figure 3.5: Raman analysis of annealed GO structures (a) Raman spectra of as-synthesized and annealed GO flakes (at 80°C for 5 days) showing the two prominent features, D and G peaks at ~1350 and ~1600 cm^{-1}, respectively. (b) Raman mapping on as-synthesized and annealed GO flakes (at 80°C for 5 days). The mapping is performed in such a way that the brightness corresponds to the ID/IG ratio. Clearly, the annealed sample is brighter and corresponds to a higher ID/IG ratio.

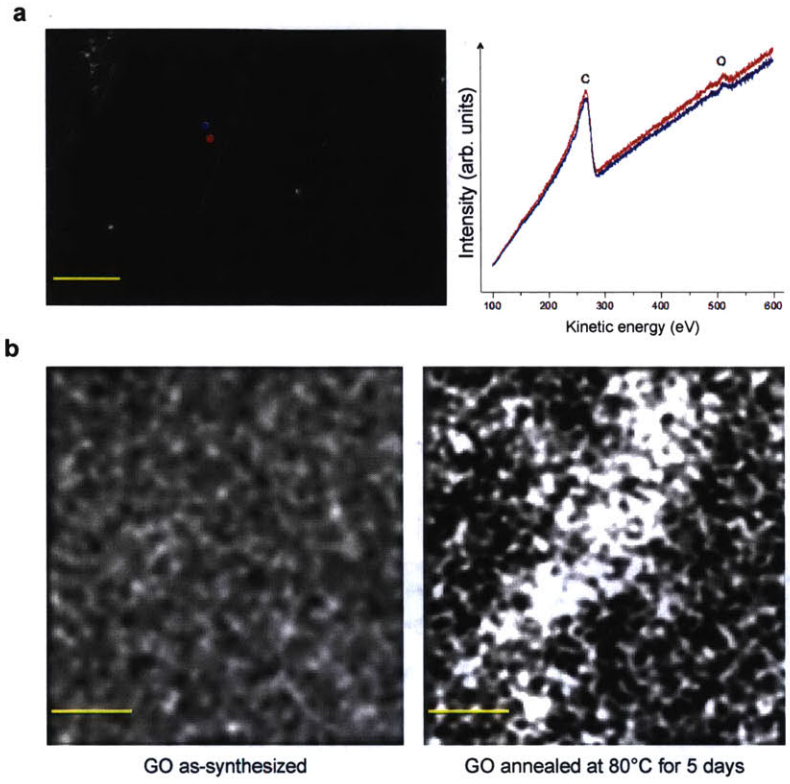

Figure 3.6: Phase separation in GO structures (a) SEM (left) and Auger electron spectra (right) of as-synthesized GO. The C and O KLL peaks at 256 and 510 eV respectively show the presence of C and O. This was confirmed at two different locations on the film as indicated in the SEM image. Scale bar, 10 μm. (b) AES oxygen mapping of as-synthesized and annealed GO films. The white spots indicate oxygen-rich regions while the black spots indicate oxygen-poor regions, or in other words, carbon-rich regions. Scale bars, 2 μm. a.u., arbitrary units.

3.3.3 Enhanced optical and electrical properties of GO through phase transformation

UV-vis absorption

The evolution of the UV-Vis absorption spectra of fd-GO samples with thermal annealing is shown in 3.7a. The as-prepared GO samples (day 0) showed typical characteristics of a main absorbance peak at ~230 nm attributed to $\pi - \pi^*$ transitions of C=C in amorphous carbon systems, and broad absorption in the visible. The main absorbance peak remained intact at ~230 nm upon annealing at both 50° and 80°C, in contrast to a clear red shift to ~260 nm reported in rGO samples [36], indicating no major reduction in covalently-bonded oxygen at these temperatures. While a weak monotonic increment in the visible absorption was recorded with increasing annealing time at 50°C, GO samples annealed continuously at 80°C became strongly absorbing in the visible, consistent with higher kinetics of phase separation at 80°C compared to 50°C. To put these results in perspective, for example, in applications involving light absorption, we estimate that this increase in absorption corresponds to a significant 38% increase in the collection of photons in the wavelength range 350-800 nm, relative to as-synthesized GO.

Electrical properties

We investigated the electrical properties of thin films prepared from annealed GO samples using four-point probe transport measurements at room temperature. As-synthesized GO samples showed high sheet resistance values indicating their insulating nature (~9×10^9 Ω/sq., comparable to 2-20 $\times10^9$ Ω/sq. reported previously [38]). Interestingly, in the case of films prepared from fd-GO samples, strong re-

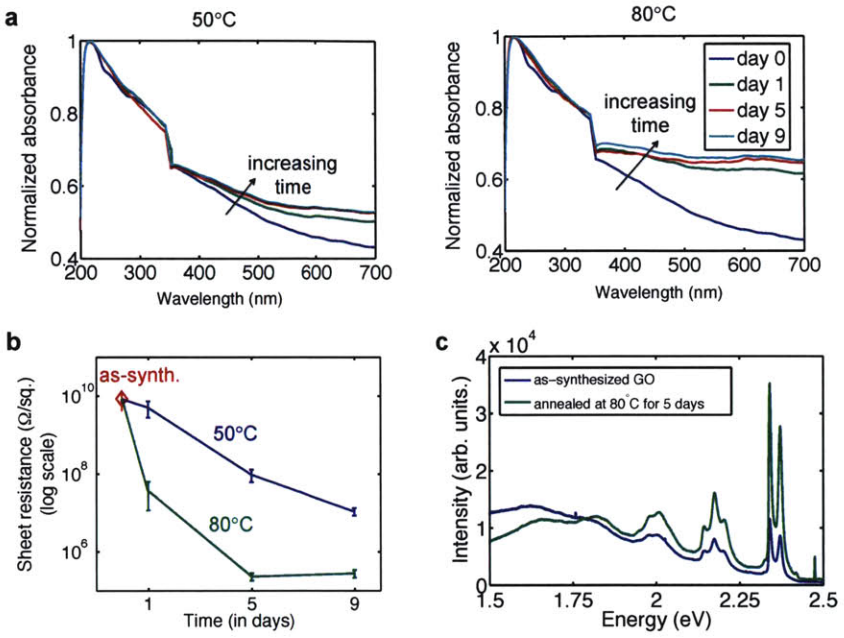

Figure 3.7: Enhanced optical and electrical properties of annealed GO (a) Normalized UV-Vis absorption spectra of fd-GO samples aged at 50 and 80°C at different time intervals showing increasing visible absorbance with thermal annealing. The bump near 360 nm is due to the change of detectors (from visible to UV). (b) Sheet resistance of GO thin films prepared from fd-GO samples annealed at 50 and 80°C, showing a reduction by up to four orders of magnitude compared to the sheet resistance of the as-synthesized GO film. (c) PL measurements on as-synthesized and annealed GO thin films (day 5) clearly show enhanced PL emission in the blue region upon annealing. A new broad peak at 1.83 eV appears, while the peaks at 2, 2.17 and 2.3-2.4 eV are enhanced significantly.

duction in sheet resistance values was observed (3.7b), consistent with the gradual reduction in sheet resistance observed for GO thin films deposited on Si substrate (3.3). Significantly, low sheet resistances of $\sim 3 \times 10^5$ Ω/sq. were measured in the case of fd-GO samples annealed for 5 and 9 days at 80°C, respectively, which are four orders of magnitude lower than the resistance of the as-synthesized GO samples, indicating superior electrical characteristics of annealed GO samples. These results are consistent with stronger changes observed in the UV-Vis absorption data of fd-GO samples annealed at 80°C (3.7a). Overall, this simple annealing procedure is effective in opening up new possibilities for fabricating thin film devices with better electron transport characteristics than that afforded by as-synthesized GO, while preserving the oxygen content in GO sheets.

PL emission

Since as-synthesized GO thin films are amorphous in nature, they exhibit a weak and broad PL emission with a peak in the red region (650-750 nm). Upon annealing the thin-film at 80°C for five days, we observed a blue shift in our PL spectra measurements, as shown in 3.7c, which is attributed to the formation of distinct and confined graphene domains in GO [36, 37]. A clear enhancement in PL intensity of annealed GO samples within the energy range 2-2.5 eV can be observed from our experiments, indicating superior PL characteristics afforded by the phase transformation process.

Although previous reports have shown enhanced electronic properties of GO under relatively low-temperature annealing between 25-150°C combined with suitable chemical treatments [67, 33, 62, 68], such improvements have come at the expense of oxygen content, leading to the formation of rGO. In this work, such

control in optical and electronic properties with a simple thermal annealing procedure are obtained without a compromise in the covalently-bonded oxygen content, and without being subjected to any chemical treatments.

3.3.4 Size of graphitic domains formed upon phase transformation

We carried out additional analysis to estimate the range of domain sizes in annealed GO samples. Analogous to the case of phase separation in hybridized carbon boron nitride monolayers [69], our calculations also indicate that larger graphitic domains are thermodynamically preferred in order to decrease the number of interfaces and the associated interfacial energy between oxidized and graphitic domains (see Figure 3.8). The structure is more favorable when the number of interfaces is lower (two interfaces on the right structure compared to four on the left structure). Our preliminary observation also suggests that the interface composition has an impact on the stability of GO structures, which deserves further attention.

In order to understand the structural evolution of GO upon annealing, we first note that the as-synthesized GO structure consists of two distinct features: (1) small sp^2 fragments (or chains) that correspond to no specific structure, and (2) larger unoxidized graphitic domains on the order of $\sim$3 nm in size [36]. On progressively annealing GO, we expect the small sp^2 fragments to interact and coalesce (or in other words, undergo the process of phase separation) leading to well-defined graphitic domains. On the basis of Raman and PL spectra from GO thin films, we conclude that such domains are on the order of 1-2 nm and are mainly responsible for the observed blue-shift in the PL (2-2.5 eV).

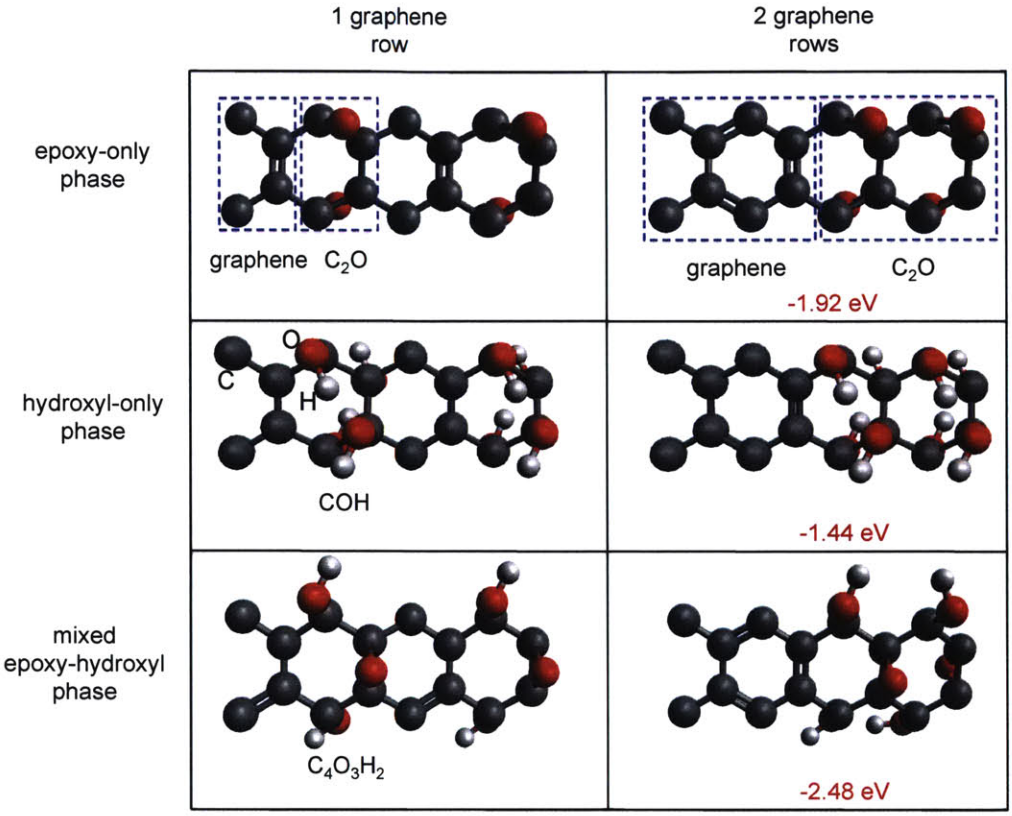

Figure 3.8: Impact of the number of interfaces on the stability of GO structures. Three different ordered phases considered in this work: epoxy-only phase (C_2O), hydroxyl-only phase (C-OH) and a mixed epoxy-hydroxyl phase ($C_4O(OH)_2$). In all three cases we observe that phase separation is favorable, i.e. structures with two graphene rows together (two interfaces) are more favorable than the structures where they are separated by the oxidized phase (four interfaces). The stability of the phase-separated structure (2 graphene rows) relative to its counterpart on the left (1 graphene row) is also reported in red text.

In parallel, it is reasonable to expect that the ~3 nm domains already present in as-synthesized GO to further grow upon annealing. We expect these domain sizes to extend from ~3 nm to tens of nanometers, similar to the range of domain sizes observed in case of carbon boron nitride monolayers [69]. DFT calculations show that such large domains formed within the sp^3-matrix open up optical gaps continuously up to 2 eV, which help explain the continuous increase in the optical absorption spectra in both the visible and the infrared [58, 36]. Further, these estimates also explain why certain regions are relatively oxygen-rich compared to other regions in our AES maps. Although formation of such larger domains on the order of tens of nanometers requires considerable diffusion of oxygen groups, we found that such mean diffusion lengths can nevertheless be achieved at the temperatures considered in this work - using the Arrhenius equation, we computed diffusion lengths and found them to be on the order of hundreds of nanometers. While we have shown these results for our as-synthesized GO samples with an oxygen content of ~30%, we expect these domain sizes to be tunable depending on the oxygen concentration, temperature and anneal time, providing additional opportunities for controlling the properties of oxidized graphene.

3.4 Appendix

3.4.1 Experimental methods

Synthesis of GO

GO was prepared from synthetic graphite powder (-325 mesh, 99.9%, Alfa Aesar, MA, USA) using the Hummers' approach [26]. The yellowish-brown filter cake

obtained was suspended in 320 mL of water, to give a GO suspension of ~0.5wt.% solids. The suspension was put in a sealed glass bottle and kept in a vacuum desiccator for long-term storage. It was observed that the stock suspension is stable at room temperature, without the addition of any surfactant.

Preparation of freeze dried GO (fd-GO) samples

In order to study the effects of long-term thermal annealing on GO alone, and discount the effects of the solvent environment, we prepared dried samples from the stock suspension. The stock suspension was diluted to 10x and 1mL of this diluted suspension was taken in several eppendorf tubes, and they were solidified rapidly by plunging into liquid nitrogen. The frozen samples were put in a lyophilizer (Labconco FreeZone 2.5 Plus, MO, USA), and kept at 0.008 mbar pressure for a day for complete extraction of the water content from the samples. These samples were stored in a vacuum desiccator.

Time-course annealing of GO samples

We studied the effects of thermal annealing on both GO suspensions and fd-GO samples. For GO suspensions, 1 mL of the 10x diluted stock solution was taken in 10 eppendorf tubes. For the fd-GO samples, the lyophilized samples were used as-is in 10 eppendorf tubes. One batch of 5 samples (both suspension and solids) was placed in a vacuum oven at 50°C, and another similar batch at 80°C. Both batches were started simultaneously at t = 0. Then, at t = 1, 3, 5, 7 and 9 days, we retrieved 1 eppendorf tube from each oven (both solid and liquid samples), and these were stored in a vacuum desiccator at room temperature for further characterization.

Characterization

UV-Vis absorbance spectroscopy. GO suspensions obtained from annealing experiments were subjected to a vigorous vortex treatment and further sonicated for 20 mins. They were then diluted to 160x (of the stock suspension) for absorbance measurements. 100 μL of sample was taken in a glass cuvette with a 1cm path length. UV-Vis absorbance was measured using a DU-800 Spectrophotometer (Beckman Coulter, CA, USA) with respect to a water (blank) baseline. The scan range was 200-1100nm, at a rate 600 nm/min. For the UV-Vis absorption measurements on fd-GO samples, we used a Cary 300 spectrophotometer (Agilent Technologies, CA, USA) with a solid state sample accessory with z-height adjustment, operating in diffuse reflectance mode. The fd-GO samples were scanned from 200-800 nm at a scan rate of 1 nm/s. The reflectance measurements were converted into corresponding absorbance data after suitable background subtraction.

4-point probe measurements. Electrical transport measurements of GO films prepared from annealed GO samples were carried out using a four-point probe technique (Model 2525, The Micromanipulator Company, NV, USA) at room temperature. GO samples were drop cast into 1cm^2 area films on an insulating glass substrate. Measurements were taken by varying the applied voltage from -1 to +1V.

Infrared spectroscopy. GO suspensions obtained from annealing experiments were freeze dried and the FTIR spectrum (800-4000 cm^{-1}) was measured using a Thermo Fisher Continuum FTIR Microscope in the transmission mode. A spot size of 100 μm was used. The transmission measurements were converted

into corresponding absorbance data and a suitable five-point baseline correction was applied to all spectra.

PL measurements. PL from the GO samples was measured using a NanoLog spectrofluorometer (HORIBA Jobin Yvon, NJ, USA). The GO samples were diluted in water to 500x of the stock concentration. A CW Xenon-lamp with a monochromator was used for the excitation source and the samples were excited at 350 nm. The fluorescence was measured in the range 400-750 nm, using a FluoroHub single photon counter (HORIBA Jobin Yvon, NJ, USA), with an integration time of 0.1 s/nm.

Thermogravimetric analysis. We characterized the thermal properties of GO by TGA (TA Instruments Q500 TGA). GO solids were initially equilibrated at 30°C for 30 mins, which was followed by a ramp up to 80°C where it was held isothermally for 9 days to record mass loss during the annealing run. Typical GO thermograms were obtained by similar equilibration, followed by a ramp up to 800°C. All measurements were taken at a nitrogen gas flow rate of 40 ml/min and ramp rate of 5°C/min was used.

Raman spectroscopy. Unpolarized Raman spectra were recorded at room temperature on GO flakes drop cast onto a Si substrate. Mapping images were acquired using Renishaw Raman / PL system with moving stage (100nm precision) using 488 nm laser source and 100x short working distance optical lens (Olympus 100x).

Nano-Auger electron spectroscopy measurements. Auger spectroscopy was performed using a field emission electron source and a multi-channel detector at ultra-high vacuum (2-5 $\times$ 10^{-10} mbar). A series of Auger spectra were measured on several different regions with a scan area of 3 μm $\times$ 3 μm. The AES scanning

was performed to detect the oxygen concentration. To eliminate the native oxide contribution on conventional substrates such as SiO_2, Si, Al_2O_3, the graphene oxide was transferred onto non-oxidizing MoS_2 substrates.

3.4.2 Computational methods

MD simulations used to prepare realistic GO structures were carried out using the LAMMPS package [53] with the ReaxFF reactive force-field, chosen here for its ability to accurately describe bond-breaking and formation events in hydrocarbon systems [44]. We employed a time step of 0.25 fs and the NVT Berendsen thermostat [8]. To assess the energetics of the phase separation process into oxidized and graphitic domains, we considered 3 $\times$ 1.3 nm periodic graphene sheets with different oxidized and graphitic domain sizes. The oxidized domains contained randomly distributed epoxy and hydroxyl groups [39, 34]. The temperature of the GO sheets was increased from 10 K to 300 K over a time interval of 250 fs. The system was then annealed at 300 K for 250 ps to allow for structural stabilization. Such MD thermal anneal runs have been previously employed to generate both GO and reduced GO structures by us and other groups [8, 38, 34].

In all the DFT calculations presented in this work, the structures were relaxed to less than 0.03 eV/Å residual atomic forces using DFT with a plane-wave basis set as implemented in the VASP package [54, 55]. We used the Projector Augmented Wave (PAW) method to describe the core electrons [56] and the Perdew-Burke-Ernzerhof exchange-correlation (XC) functional [57] in combination with a gamma-point $\vec{k}$-grid. The wave function and charge density were expanded in plane waves with a wavefunction kinetic energy cut-off of 500 eV. A vacuum region of 16 Å was

used in the direction normal to the sheets. For computing the activation energies used to determine the kinetics of oxygen diffusion, we employed nudged elastic band (NEB) calculations as implemented in VASP with $9 - 13$ image structures between the reactant and the product.

Chapter 4

Utilization of phase transformation in developing new applications

4.1 Application 1: Biosensors - Enhanced cell capture efficiencies through phase transformation in GO

A sensor is a transducer whose purpose is to sense some characteristic of its environs. An important aspect of a sensor is to be able to detect with high sensitivity. There are many examples of sensors: temperature sensors, pressure sensors, chemical sensors, biosensors etc. In this thesis, we study a particular class of biosensors, which are used to not only detect specific cellular components present in human blood, but also capture and isolate them from other components.

4.1.1 Importance of biosensors and current challenges in this field

Human blood consists of mainly red blood cells (RBCs), white blood cells (WBCs) and platelets. WBCs in particular carry information about a patient's immune system and can be useful to obtain a wealth of knowledge about the patient's health. In this work, we study the problem of detecting and isolating WBCs and its subpopulations from blood. An important challenge in doing so is to be able to design a system that could be sensitive to WBCs. This is done by using a class of antibodies that can specifically capture necessary subpopulations of WBCs [70, 71]. However, these antibodies need a template (or a substrate) to be anchored onto. Traditionally, microfluidic devices have been used to capture and isolate different types of cells [72]. These devices rely on three-dimensional microstructures, trapping arrays and microfilters, that have been useful in isolating cell components. However, such three-dimensional systems suffer from problems such as cell trapping, issues with recovery and imaging, limitations with downstream analysis and further cell culture, complex and expensive fabrication at the micro-nano scale [72, 73, 74, 75].

4.1.2 Role of GO and phase transformation in GO toward addressing these challenges

Two-dimensional materials such as GO can overcome these limitations due to their high surface to volume ratio. They are essentially flat nano sheets, their synthesis procedures are straightforward, inexpensive and well established [6]. They can be deposited on a wide variety of substrates from a solution, with excellent control

over the thickness of the sheets from micron-scale down to a monolayer. The most important aspect of GO is its rich oxygen and carbon framework, whose functionalization chemistries are well-established. With all these advantages, it has been envisioned and demonstrated that GO sheets can be powerful templates for designing cell capture assays.

A particular example for constructing a biosensor assay using GO nanosheets for sensitive capture of circulating tumor cells (CTCs) was reported recently by Yoon *et al.* [73]. They demonstrated the utility of GO sheets to form nanometer-thick films on a patterned gold substrate, which were then functionalized with phospholipid-polyethylene-glyco-amine (PL-PEG-NH_2). After other surface treatments, the CTCs were captured by subsequent NeutrAvidin and biotinylated Ep-CAM antibody interactions. CTCs were captured with high sensitivity at a low concentration of target cells (73$\pm$32.4% at 3-5 cells per ml blood). The procedure demonstrates high sensitivity towards capturing CTCs and also provides an initial step towards better imaging and possibility of additional downstream analysis and cell culture.

Although the capture yield is 73% in the above procedure, there is large room for improving the device characteristics. The standard deviation is high, which could be bottleneck when it comes to reliable detection and the extent of cancer in patients. Complex gold patterns were necessary to improve the capture yield, without which the efficiency was $\sim$40%. Finally, little attention was given to the chemistry of GO functionalization at the nanoscale. We believe there could be additional benefits to controlling the functionalization at the nanoscale, which can then translate into improved cell capture at the micron scale.

In what follows, we show the role of tailoring functionalization of GO at the

nanoscale in improving the cell capture yield at the macro scale. We do so by using the concept of phase transformation developed in Chapter 3. As an example system, we use the VHH7 antibodies to capture a particular subpopulation of WBCs, i.e. Class II MHC-eGFP+ cells. This work was done in collaboration with Prof. Guan-Yu Chen (National Chiao Tung University, Taiwan), Prof. Angela Belcher (Koch Institute, MIT) and Prof. Hidde Ploegh (Whitehead Institute, MIT).

4.1.3 Cell capture using phase transformation in GO

Sample preparation

Schematic illustration of antibody (VHH7)-based GO substrates for capture of Class II MHC-eGFP+ cells from whole blood is shown in Figure 4.1. Glass slides are coated with 3% (3-aminopropyl)triethoxysilane (APTES) in toluene for 30 minutes and washed with toluene, ethanol, and then water. Following washes, slides are immersed in a GO (1 mg/ml) suspension for 1 hour. GO-coated slides are then annealed at 80°C in a temperature-controlled oven to facilitate phase transformation in GO as described in Chapter 3. We then remove GO slides at regular intervals to have day 0 (control, as-synthesized GO samples), day 1, 5 and 9 (phase transformation-induced) samples. Day 0-9 allows us to monitor the effect of different degrees of phase transformation on functionalization and subsequent cell capture.

For each of the glass slides, a diamino-polyethylane glycol (NH_2-$(PEG)_5$-NH_2) linker is introduced with one end reacting with GO sheets. The reaction mainly occurs with the epoxy groups present in GO sheets [76]. In order to improve the

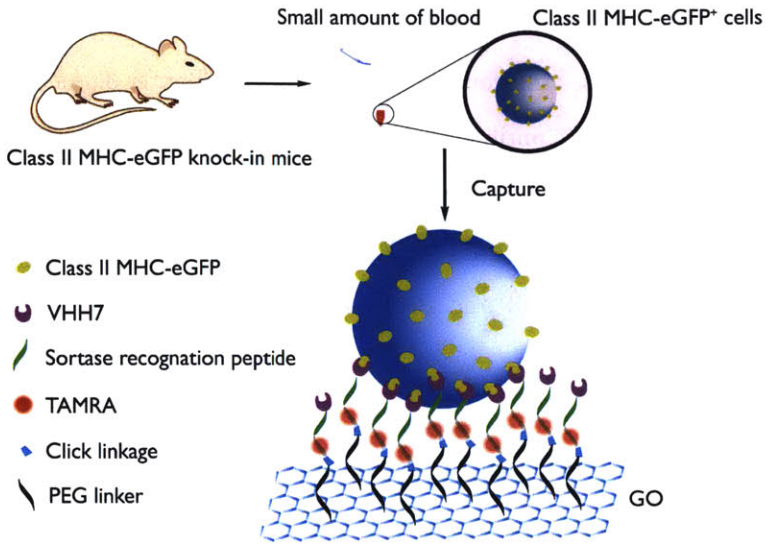

Figure 4.1: Schematic illustration of antibody (VHH7)-based GO substrates for capture of Class II MHC-eGFP+ cells from whole blood.

reactivity of the carboxylic groups in GO toward the -NH_2 linker, we activated them with N-hydroxysuccinimide (NHS) in a reaction catalyzed by 1-Ethyl-3-(3- dimethylaminopropyl)carbodiimide hydrochloride (EDC). This ensures a large number of -NH_2 linkers to be bonded to GO. The other end of the PEG linker is further functionalized with an NHS-activated dibenzocycolctyne (DBCO). The antibody protein, which has been labeled with an azide in a sortase-catalyzed reaction, is then clicked onto the DBCO in a strain-promoted cycloaddition.

The VHH7-GO functionalized slide was assembled with a second glass slide to form a cell capture chamber. Two strips of double-sided tape served as spacers to yield a chamber of approximately 12 mm $\times$ 25 mm $\times$ 0.1 mm for a total volume of $\sim$30 μL. The VHH is thus directly attached to one of the surfaces of the capture chamber. Assembly of this device requires no more than two-sided tape

and a second, unmodified glass slide. Delivery of ~30 μL of whole blood or a cell suspension is then achieved by contacting the opening of the chamber with the tip of a mechanical pipetting device. Within seconds, discharge of the intended volume then fills the chamber by capillary action. Wash steps are conducted in similar fashion by delivery of buffer to one open side of the chamber, and wicking off buffer at the opposite end of the chamber, using filter paper to ensure flow across the chamber surfaces.

Improved cell capture performance of biosensor through phase transformation

We first tested the performance of VHH7-modifed GO substrates using cell lines (Figure 4.2). Mouse B lymphoma (A20) and human B lymphoma (Raji, murine Class II MHC-negative) cell lines were labeled with a fluorescent cell tracker dye, diluted in PBS and loaded into the VHH-GO device for 10 min at room temperature. A cell density of 2×10^5 was used to test the performance. We observed increasing cell capture efficiencies with annealing time, indicating that mildly annealed, phase transformed GO substrates improve the device performance. The control cases, i.e. without VHH7 showed negligible cell capture, indicating the specificity of VHH7 toward capturing A20 cells.

We further tested the performance using whole blood samples (Figure 4.3). Fresh blood was obtained from Class II MHC-eGFP knock-in mice for ready visualization of Class II MHC+ cells by their GFP (green fluorescent protein) fluorescence. Analysis of Class II MHC-eGFP+ cells showed an average capture efficiency of 54 $\pm$ 3% on the VHH7-functionalized nanosubstrate for the day 0 case (~11,000 cells). With the day 9 sample, the cell capture efficiency increased to 92 $\pm$ 7%

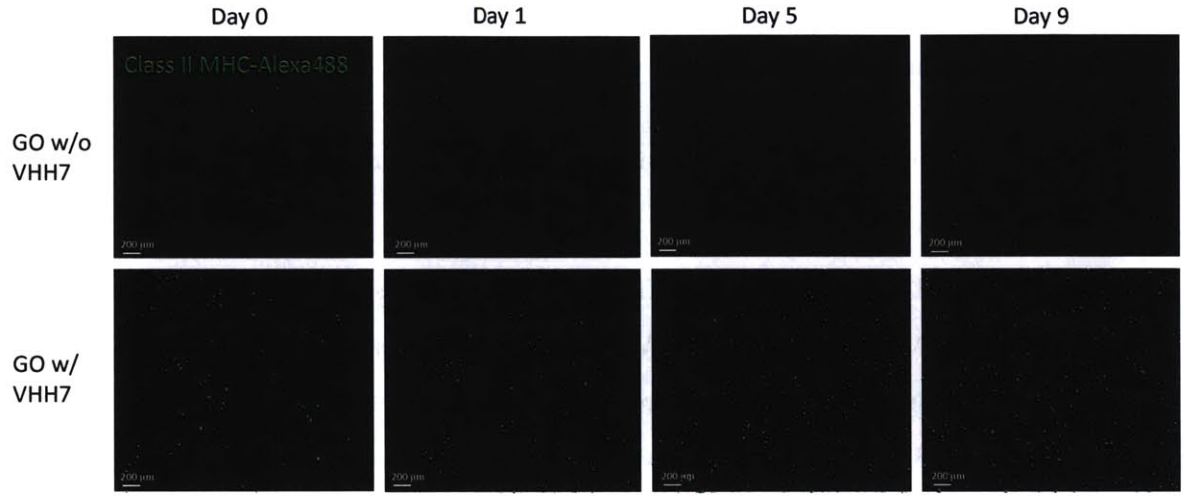

Figure 4.2: Quantification of cell capture on GO substrates using A20 cell lines. Quantification of captured A20 cells (murine Class II MHC+) on GO substrates containing the control sample (day 0), and with mild annealing (day 1-9). The cells are stained with Alexa488 cell tracker dye which shows green fluorescence during confocal imaging. Since we are interested in imaging cells, which are on the order of 1-10 microns, a micron-scale resolution is chosen. Each green spot represents a captured cell. It is clear that the cell capture number increases with mild annealing time. Samples without VHH7 are also shown, indicating negligible capture without the presence of antibodies.

compared to the day 0 sample, once again indicating its superior performance and the positive impact of the phase transformation induced in GO. Conversely, without VHH7, negligible number of cells were retained, in agreement with what was observed with the A20 cell line.

It should be noted that these experiments were carried out at room temperature and achieving a capture efficiency of 92% is significant at room temperature. This avoids the use of an incubator to increase the temperature to 37°C and further helps maintain a steady state temperature during the entire process - from device fabrication to cell capture. Also, if people plan to use this device as a commercial kit or Point-of-Care Testing in the future (for example, using this at home), this would be an added benefit since cell capture can be performed by patients in-house at ambient conditions.

We also performed additional characterization of the captured cells through staining with DAPI. Since DAPI is a nuclear stain, it stains non-specific cells as well, thus enabling us to compare with eGFP+ cells to quantify and characterize non-specific binding. The results of this experiment performed on the best case (day 9) are presented in Figure 4.4. The top panel essentially reveals minor quantities of non-specific binding (B, T cells etc.), indicated by DAPI +/eGFP -/, thus suggesting that phase transformation doesn't lead to undesirable characteristics (such as non-specific capture). We can further confirm from GFP signals that the captured cells were MHC class II, which only expressed florescence on the cell surface (bottom panel of Figure 4.4). In addition to small non-specific binding, these results show that the captured cells are available for further staining and analysis.

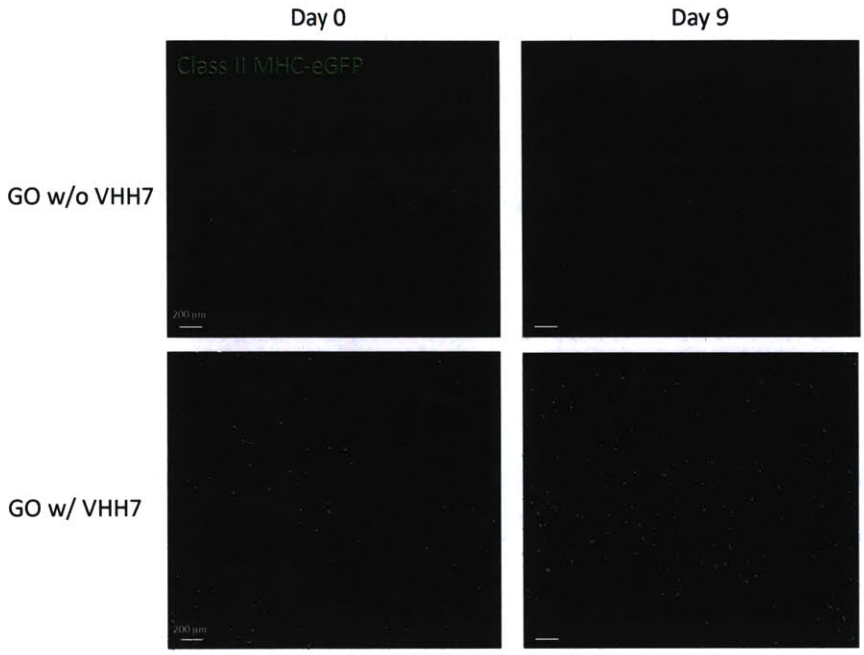

Figure 4.3: Quantification of cell capture on GO substrates using Class II MHC-eGFP+ whole blood samples, performed at room temperature. Quantification of captured eGFP+ cells comparing day 0 and day 9 cases. In this case, the GFP (green fluorescent protein) markers that are expressed by the captured cells are used to identify them under a confocal microscope. Clearly, the day 9 case shows a higher cell capture efficiency ($92 \pm 7\%$) compared to the day 0 case ($54 \pm 3\%$). Samples without VHH7 are also shown, indicating negligible capture without the presence of antibodies.

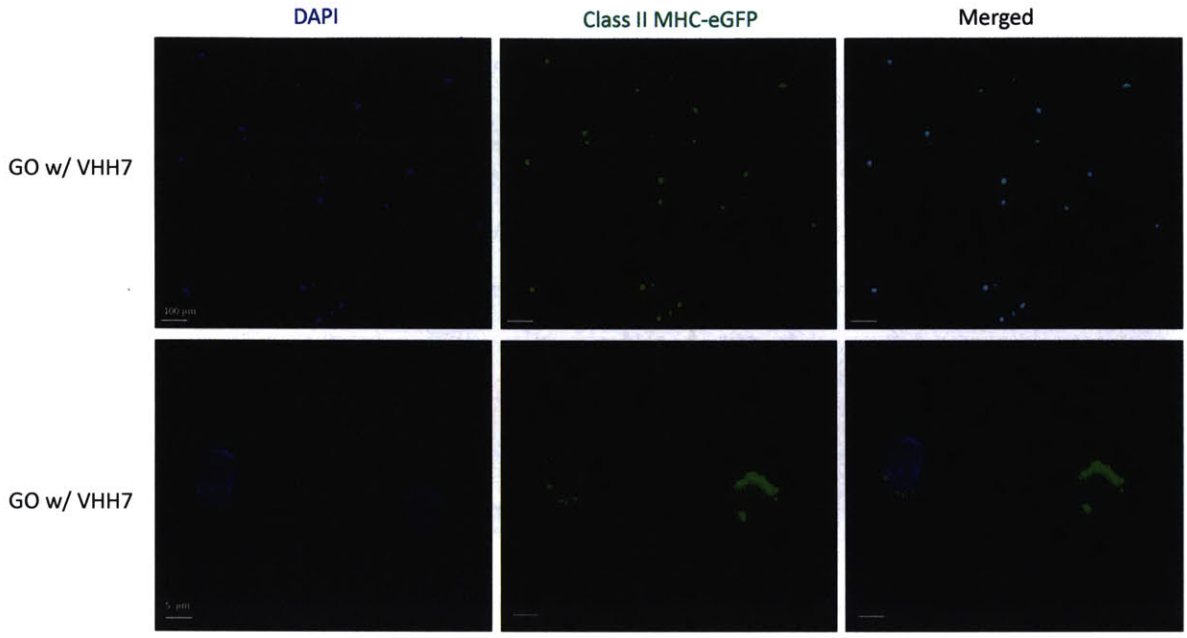

Figure 4.4: Additional characterization of captured Class II MHC-eGFP+ cells. (Upper panel) Captured cells were stained with DAPI and the results are compared with eGFP+ cells. DAPI is a nuclear stain that enables visualization of all the WBCs, while GFP enables visualization of the specific Class II MHC cells. Therefore, by combining the two images, a DAPI +/eGFP -/ signal indicates non-specific cells captured during our experiments. These results show that non-specific binding is small. (Lower panel) eGFP+ cells express florescence on the cell surface, thus indicating that the captured cells are indeed MHC class II.

Enhanced antibody (VHH7) grafting onto GO nano sheets through phase transformation

In order to understand the reasons behind enhanced cell capture of phase transformed GO, we conducted additional experiments. We envisioned that the enhanced cell capture could be a result of improved antibody grafting onto the GO substrates. In order to verify this hypothesis, we assessed the concentration of antibodies bound on the GO substrate. We engineered a sortase-ready version of VHH7 with an LPETG motif near the C-terminus. Using standard sortagging protocols we introduced a Gly peptide equipped with a TAMRA fluorophore and an azide, to partner with the DBCO moiety during the click reaction. Figure 4.5 shows confocal images obtained on the sample set (from day 0-9). The results exhibit a clear increase in the florescence intensity and distribution from day 0 to day 9 samples, confirming greater concentration of antibody grafting on to the GO substrates that have undergone phase transformation.

Characterization of the GO/NH_2-linker interface

It is well known that the majority of the NH_2-linkers bind covalently to GO through the epoxide ring opening mechanism on the basal plane (Figure 4.6) [76]. In this mechanism, the epoxy ring opens and the dangling carbon attaches to the N atom of the amine group [77]. One of the H atoms of the NH_2 group attacks the oxygen atom, leading to the formation of the -OH bond. An additional reaction is the the attachment of NH_2-linkers to the minority -COOH groups at the sheet edges. Usually, since the -COOH groups are acidic, the reaction leads to equilibrium between alkyl-ammonium ions (NH_3^+) and -COO^- groups.

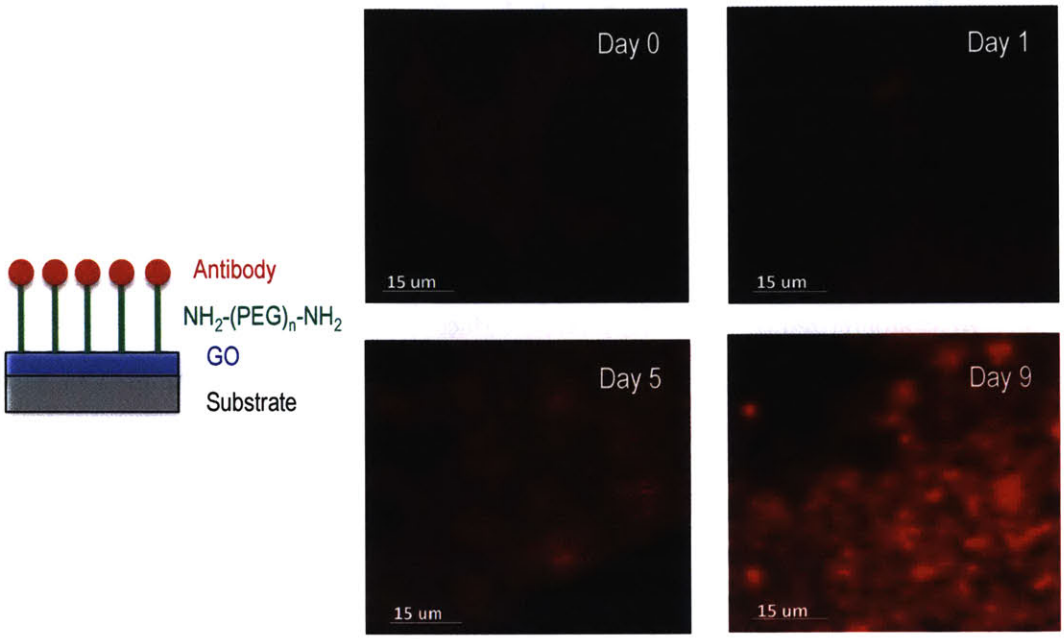

Figure 4.5: Quantification of the number of antibodies grafted onto the GO substrate. Antibodies are equipped with TAMRA flourophore and thus can be visualized under a confocal microscope. The plots reveal increasing florescence with time of annealing, indicating denser grafting of the antibodies on to the GO substrate. A simple schematic of the system is also shown on the left.

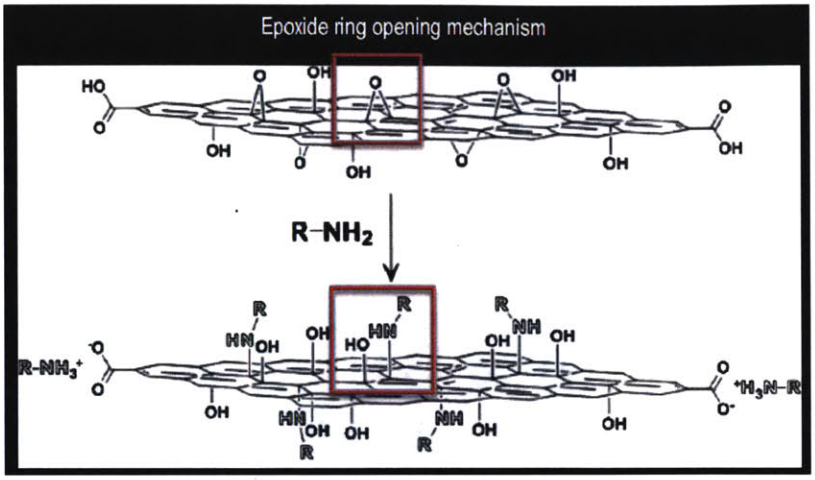

Figure 4.6: Schematic of the epoxide ring opening mechanism which leads to the formation of covalent bonding between GO and NH_2-linkers (taken from Ref. [76]).

We characterized the GO/NH_2-linker interface using XPS measurements. Representative N 1s spectra obtained from day 0-9 samples are shown in Figure 4.7a. The N 1s spectrum can be deconvoluted into three peaks: C-N peak (399.7 eV), C-NH_3^+ peak (401.8 eV) and a shoulder at 398.3 eV representing unchelated or physisorbed linkers [76, 78, 79]. The N 1s spectra seem to become narrower and sharper with peak at 399.7 eV with annealing time as seen. We calculated the C-N bond fraction which is observed to increase with annealing time, from ~70% in day 0 to ~90% in day 9 (Figure 4.7b), thereby indicating an increase in the covalent bonding of the NH_2-linkers with GO nanosheets. The N atomic percent was also obtained from the XPS analysis, which showed slight changes with annealing time. However, quantification of N content at such small quantities (3-4 at%) is generally unreliable. These results indicate that the increasing number of antibody grafted onto GO correlates with the C-N bond concentration, thus suggesting that the C-N bond is crucial toward building an efficient biosensor.

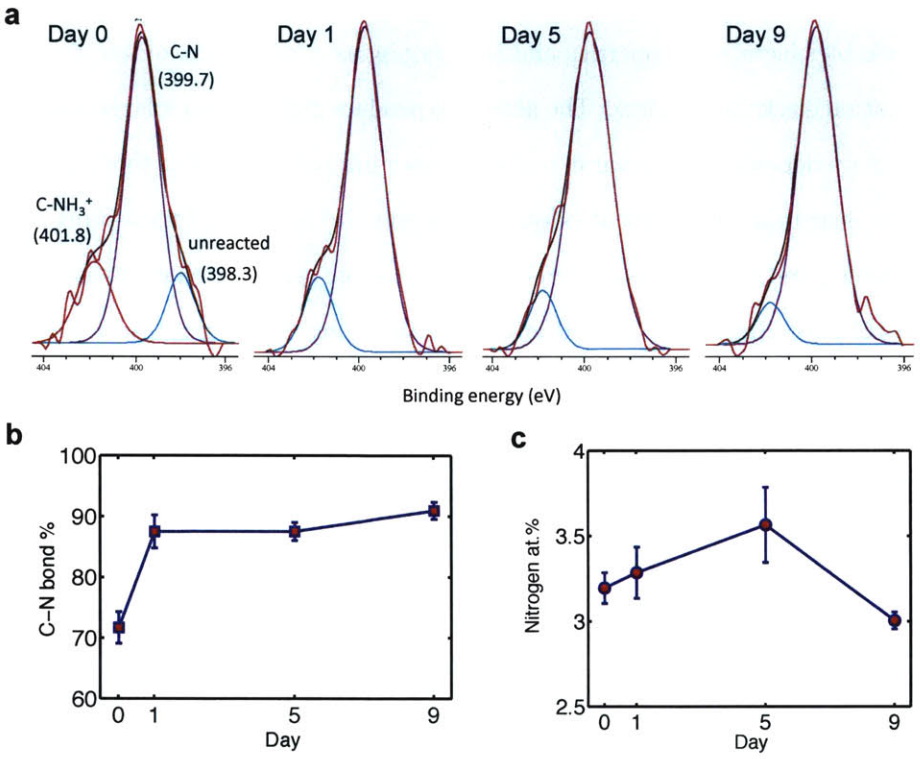

Figure 4.7: Structural models comparing rGO obtained from direct reduction of GO to that obtained after including the pretreatment step (mild annealing). The upper panel illustrates the formation of distinct graphitic domains in GO structures after the mild annealing, as demonstrated in Chapter 3. The graphitic domains are represented by orange, while the oxidized domain is represented by grey. The bottom panel shows the corresponding rGO structures obtained after thermal reduction. The treated-rGO structure illustrates larger sp^2 clusters compared to the control sample, which could lead to better electrical properties of rGO thin films.

4.2 Application 2: Preparation of graphene thin films with better electrical properties

As noted in Chapter 1, graphene is an atom-thick sheet of carbon possessing remarkable electronic properties and is emerging as a leading candidate for next-generation electronic devices. The ability to produce graphene on a large scale and control its deposition on a variety of substrates has been crucial in this regard. It is now clear that the chemical exfoliation of graphite to form solution-processable GO sheets, and their subsequent reduction to restore graphitic characteristics and form rGO (or chemically derived graphene) thin films is a promising step in this direction [9].

4.2.1 What are the limiting factors of rGO produced under current protocols?

rGO obtained under current thermal reduction protocols contain randomly distributed residual oxygen of 5-8 atomic percent (at%) in the form of thermodynamically stable carbonyl and ether groups, a factor that still remains uncontrolled at a given reduction temperature [8]. In addition, the generation of carbon vacancies during the reduction process, and their spatial distribution in the graphene lattice restricts the expansion of the sp^2 phase, resulting in inferior electrical properties of rGO compared to mechanically exfoliated graphene [28, 80]. Given such a fundamental limitation toward the improvement of electrical and structural properties of rGO sheets, it is of utmost importance to develop strategies that enable control over oxygen removal and render larger sp^2 clusters that are minimally disrupted

by sp^3 sites or carbon vacancies.

4.2.2 Strategy to produce rGO sheets with better electrical properties

We envisioned that our mild annealing procedure at 80°C could be used as a pretreatment step toward the production of rGO thin films. This is because annealing at 80C leads to the expansion and development of distinct graphitic domains in GO. If this procedure is followed by a high temperature annealing or chemical reduction step, the rGO films thus produced would contain larger sp^2 domains compared to rGO films obtained through direct reduction of GO. This idea is illustrated in Figure 4.8 using structural models for GO and corresponding rGO structures. Thus, the rGO films produced using the pretreatment step could lead to better electrical characteristics due to increased sp^2 domain sizes.

In order to test this hypothesis, we performed electrical transport measurements on rGO thin films and the results are discussed in detail below.

Sample preparation

Figure 4.9 shows a schematic of the experimental procedure used in our study. GO solutions were synthesized using the Hummers method detailed in the appendix of Chapter 3. Two types of thin films were tested: 1) GO produced through drop-casting onto clean Si substrates, and 2) Free-standing GO thin films produced through the vacuum filtration technique. Both these thin films were dried at least for 12 hours at room temperature. The films were subjected to mild annealing at 80°C in a temperature-controlled oven for a course of nine days to facilitate

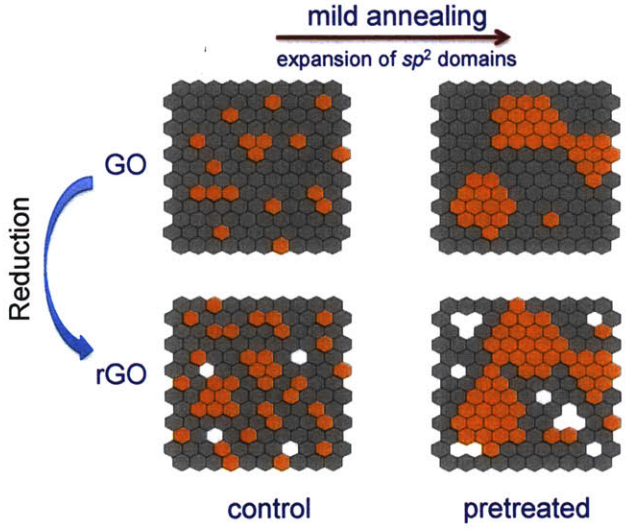

Figure 4.8: Structural models comparing rGO obtained from direct reduction of GO to that obtained after including the pretreatment step (mild annealing). The upper panel illustrates the formation of distinct graphitic domains in GO structures after the mild annealing, as demonstrated in Chapter 3. The graphitic domains are represented by orange, while the oxidized domain is represented by grey. The bottom panel shows the corresponding rGO structures obtained after thermal reduction. The treated-rGO structure illustrates larger sp^2 clusters compared to the control sample, which could lead to better electrical properties of rGO thin films.

the expansion and development of sp^2 domains, which we hereafter refer to as 'pretreatment'. Samples were retrieved at intervals of one, five and nine days, to obtain GO samples with varying degree of sp^2 clustering with the day 0 sample showing no clustering, while the day 9 sample showing the greatest degree of clustering as demonstrated in Chapter 3. The retrieved thin-film samples were thermally reduced by placing them at elevated temperatures (250°C, 350°C and 450°C) in a temperature-controlled oven for 20 minutes.

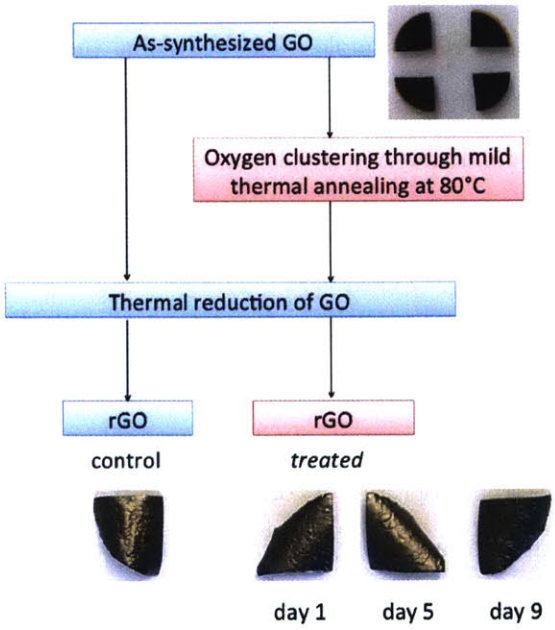

Figure 4.9: Schematic of the experimental procedure employed. As-synthesized GO structures were subjected to a mild thermal annealing treatment at 80°C for nine days to facilitate different degree of oxygen clustering, followed by their thermal reduction at elevated temperatures to obtain treated-rGO structures. The control rGO sample was obtained by directly reducing the as-synthesized GO film as depicted. Example GO and rGO free-standing thin films are shown.

Electrical measurements

We evaluated the electrical properties of rGO thin films using four-point probe transport measurements, conducted at room temperature. Figure 4.10a compares the sheet resistance values of control rGO films (day 0) with those of the treated-rGO films, for thermal reduction temperatures of 250 and 350°C. In agreement with our hypothesis, we did observe a sharp drop in the sheet resistance values with pretreatment time at these reduction temperatures. Electrical measurements reveal 30-50% reduction in the sheet resistance values of the treated-rGO films, compared to the control rGO sample. Our additional thermal reduction experiments carried out at 450°C resulted in sample lift-off and were not suitable for sheet resistance measurements. Figure 4.10b shows a similar experiment performed on free-standing GO thin films. Consistent with the case of drop-casted GO, we observed a drop in the sheet resistance values (20-40%). The change in the sheet resistance values was gradual in this case in comparison with the drop-casted GO case.

Although the structural evolution of GO under mild annealing shows gradual change in properties, the properties of corresponding rGO structures obtained by high temperature thermal annealing rather saturate after day 1 - day 5. We attribute this to the fact that high thermal energy during reduction can disrupt the distinct sp^2 and oxygen clusters, thereby losing the effect of sp^2 clustering. Although this could be the case, we still find reduction in sheet resistance values and thus conclude that using a pretreatment step prior to thermal reduction enhances the electrical properties of rGO, compared to directly reducing as-synthesized GO that is the current standard. This possibly highlights the importance of creating

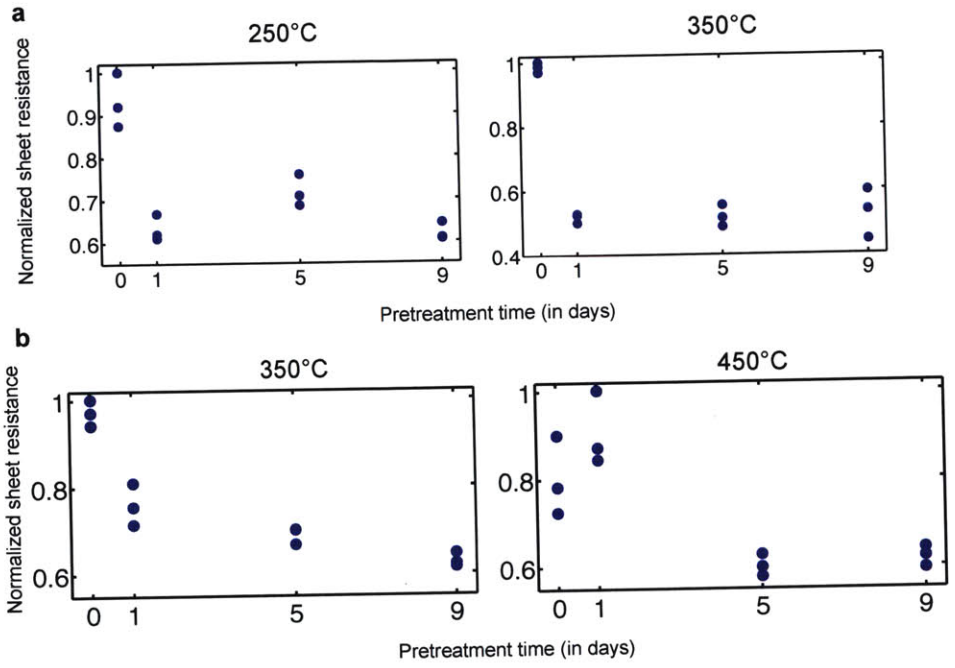

Figure 4.10: Electrical characterization of treated-rGO thin films and comparison with the control rGO sample. (a) Sheet resistances of treated-rGO thin films prepared by the drop-casting technique show reduction by up to 30-50% compared to the sheet resistance of the control rGO sample (day 0). The reduction temperature is shown above each plot. (b) Similar trends were observed for free-standing rGO thin films.

larger sp^2 clusters in enhancing the electrical quality of rGO films, a result distinct from previous studies where improvements in sheet resistance are obtained solely through oxygen removal [6, 28].

Structural evolution of treated GO structures

In order to understand the impact of sp^2 (or oxygen) clustering on the structural and chemical evolution of GO thin films at the atomic scale, we carried out a combination of classical MD simulations and DFT calculations. For our MD simulations, model GO structures with different sizes of oxidized and graphitic domains (none, three and six graphene rows) were prepared with the oxygen concentration kept fixed to mimic the oxygen clustering process (Figure 4.11a), similar to models described in Chapter 3. Briefly, the oxidized domains consisted of randomly distributed epoxy and hydroxyl groups attached to both sides of the graphene sheet [39]. Different oxygen concentrations (10 and 20 at%) and fraction of epoxy to hydroxyl groups (3:2 and 2:3) were tested to study the effect of such local variations on the reduction behavior of GO films. A 3 $\times$ 1.3 nm periodic graphene sheet was used for all simulations. We used 10 samples for each composition, which allows us to present meaningful averages of the computed properties. Thermal reduction simulations were carried out at 1500 K using methods described in the appendix of Chapter 2.

The number of oxygen and carbon atoms removed from the GO structure during thermal reduction is shown in Figure 4.11b as a function of different graphitic domain sizes (in other words, as a function of increasing oxygen clustering). At high oxygen contents, our results show that not only does the number of oxygen atoms removed increase, but also the number of carbon atoms removed from the

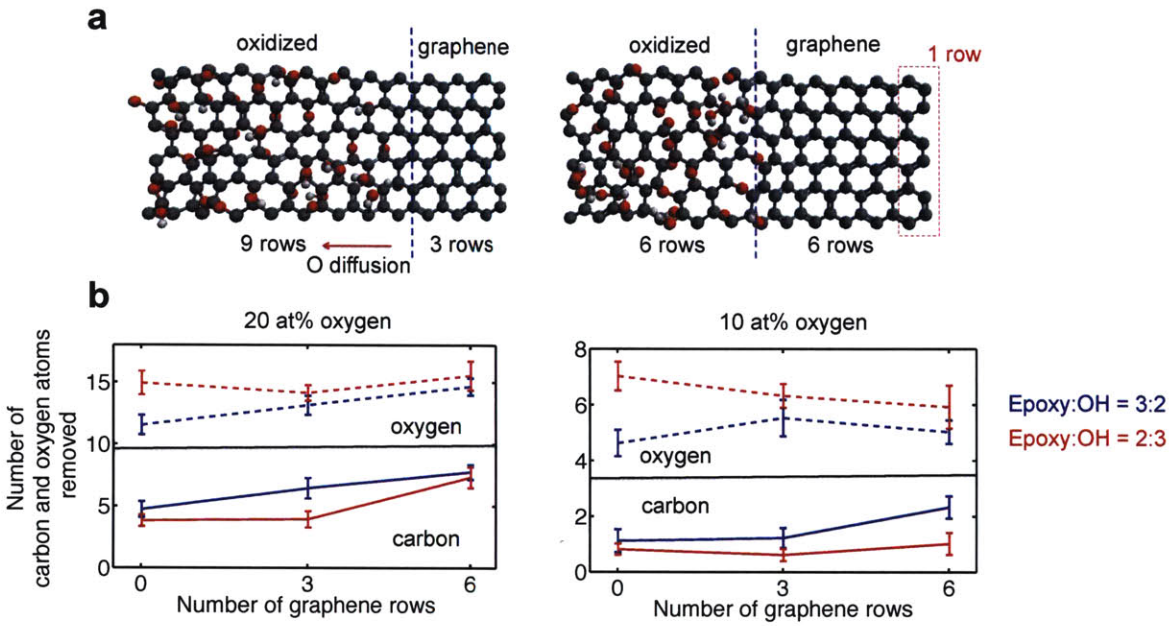

Figure 4.11: Structural evolution during the reduction of treated GO thin films. (a) Representative model GO structures used to study the effect of oxygen clustering on the thermal reduction behavior of GO structures in MD simulations. Each structure consists of two distinct oxidized and graphene phases with different domain sizes, mimicking different degrees of oxygen clustering caused by oxygen diffusion. Carbon, oxygen and hydrogen are represented as grey, red and white spheres, respectively. (b) The number of oxygen and carbon atoms removed during thermal reduction, both showing an increasing trend with increasing number of graphene rows (or increasing degree of oxygen clustering). Although the effect still persists, it is weaker for the case with lower oxygen concentration (10%).

graphene backbone increases with increasing degree of sp^2 (or oxygen) clustering. At lower oxygen contents, i.e. 10%, we observed that the sp^2 clustering has weaker effects on increasing the carbon and oxygen removal, although the effects still persist. Taken together, our results demonstrate that controlling the degree of oxygen clustering in GO structures can be an effective way to not only enhance the electrical properties, but also to tune the local residual oxygen and carbon content in the corresponding rGO structures.

Our simulations also point toward other interesting results. We found that the formation of pores (a cluster of carbon vacancies) decorated with oxygen atoms at the periphery, becomes increasingly favorable with oxygen clustering, which represents a useful control parameter for the design of next-generation graphene-based porous membranes [81, 17, 16]. Our simulations also show that epoxy-rich GO domains are more influenced by oxygen clustering, and tend to lose more carbon and oxygen atoms compared to the hydroxyl-rich domains, thereby highlighting the importance of the functional groups and providing additional guidelines for designing efficient reduction protocols.

To further understand unit processes favoring oxygen removal in addition to the consumption of the carbon backbone, we carried out DFT calculations of the reaction pathways that lead to the reduction of GO. Specifically, we considered removal of (1) O_2 (2) CO and (3) CO_2 molecules from the initial GO structures; the last two being responsible for the consumption of the carbon backbone [30]. The initial GO configurations were constructed with one (1-O), two (2-O), three (3-O) and four (4-O) neighboring oxygen atoms to model different degrees of oxygen clustering, as shown in Figure 4.12a. Only epoxy groups are considered to model these unit reactions in order to get a basic understanding of the effect of oxygen

clustering. The generation of O_2, CO and CO_2 molecules from each of these configurations was studied leading to different product structures.

We assessed the favorability of the reactions by computing the energy difference between the final and initial configurations, as shown in Figure 4.12b. First, we note that oxygen removal in the form of an O_2 molecule is diffusion-limited in the case of isolated oxygen atoms (1-O case, no clustering), i.e. oxygen atoms have to diffuse around and find a neighboring oxygen atom to form an O_2 molecule. Instead, upon partial clustering (2-O case), the formation of an O_2 molecule is no longer diffusion-limited, and removal of oxygen in the form of O_2 is favored thermodynamically by a reduction in the total energy of 1.44 eV. On the other hand, removal of oxygen through the other two reaction channels, i.e. in the form of CO and CO_2 molecules, remains thermodynamically unfavorable in the 1-O and 2-O cases.

Upon further clustering of oxygen (3-O and 4-O cases), competing reaction channels that generate CO and CO_2 molecules are favored more than O_2 evolution. These reactions consume the carbon backbone, and leave behind defects (single vacancies and holes) in rGO films. The surrounding oxygen atoms help saturate the carbon dangling bonds created due to a carbon vacancy, which explains why these reactions become favorable with increasing degree of oxygen clustering [30].

It should be noted that while our combined DFT and MD studies help interpret structural evolution at the atomic scale, they do have certain limitations. A high degree of oxygen clustering has been shown to lead to complex reconstructions in GO structures [30]. Hence, modeling realistic GO structures with a high degree of oxygen clustering is challenging and may additionally involve processes such as oxidative cutting forming graphene quantum dots [31], charring [82] and genera-

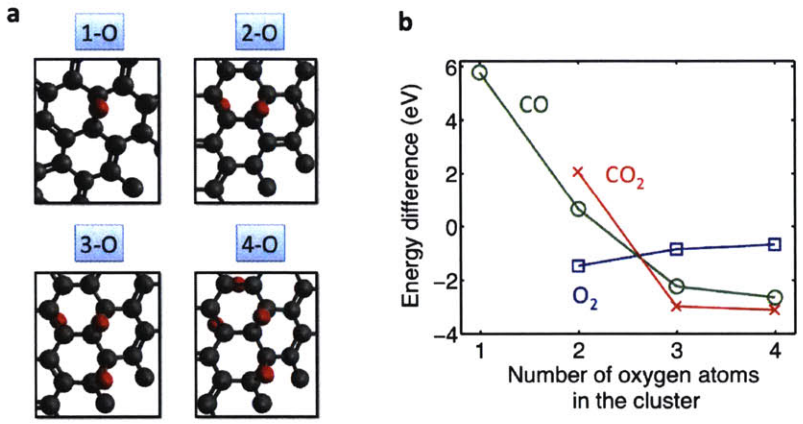

Figure 4.12: Assessing the favorability of unit reduction reactions with increasing degree of oxygen clustering using DFT calculations. a) Initial configurations with one, two, three and four neighboring oxygen atoms used to model reduction reactions. b) The energy differences (in eV) between the final and the initial configurations (E_f - E_i) listed for three reactions removal of O_2, CO and CO_2 from the initial configurations shown in (a). These results show that with increasing clustering of oxygen, removal of both oxygen and carbon in the form of CO and CO_2 becomes increasingly favorable, thereby leading to the consumption of carbon backbone and leaving behind vacancies (and holes).

tion of by-products other than CO and CO_2 as observed in the case of amorphous carbon systems [83, 84]. Recent ab initio and MD simulations based on ReaxFF potentials have predicted the evolution of small-molecule hydrocarbons (CmHn) and other molecular fragments containing oxygen (C_mH_nO) alongside CO and CO_2, when carbon-based phenolic resins are heated [82, 83, 84]. While such finer details are not captured in our simulations owing to simpler initial configurations, they nevertheless provide important topics for future exploration. Yet, utilizing the subset of rGO structures considered here, we are able to gain important understanding related to the effects of oxygen clustering on carbon and oxygen removal from GO.

Chapter 5

Conclusions and Outlook

In this thesis, we use a combination of computational and experimental techniques to understand the structure and properties of a key two-dimensional carbon-based material, called graphene oxide (GO). Based on our thorough understanding of the impact of oxygen functionalities on the sheet properties, we discover a new phase transformation mechanism in GO, which retains the oxygen content and modifies the structure of GO. The modified GO structure is shown to be advance two key applications: 1) GO-based biosensors, and 2) Reduced GO for transparent conducting electrodes. In what follows, we summarize the main findings of this thesis and provides an outlook of the utility and applicability of GO structures.

First, we employed a computational approach combining classical MD simulations and DFT calculations to simulate realistic GO and rGO structures, and relate their atomic scale structure to their sheet properties. In particular, we decomposed the contributions of individual functional groups to the stability, work function, electronic structure, and PL emission of rGO. Our results highlight the significant tunability of the optical and electronic properties of rGO, including

variation of the work function by up to 2.5 eV in structures with a precise control of oxygen-containing functional groups, and significant changes in the DOS and related PL emission by changing the ratio of epoxy to carbonyl groups. Our calculations indicate the metastable nature at room temperature of carbonyl-rich rGO structures usually obtained in the experiment, and show the favorable energetics for their conversion to hydroxyl-rich structures with lower oxygen content, driven by the carbonyl to hydroxyl conversion near carbon vacancies and holes. Our results strongly suggest that further efforts are necessary in controlling the content of individual functional groups in rGO to fully take advantage of its outstanding potential for functional devices.

Based on our understanding of the atomic structure, we demonstrated a new phase transformation mechanism in GO at mild annealing temperatures (50-80°C). Our experimental and computational results show that the phase separation of the mixed sp^2-sp^3 hybridized GO phase into prominent oxidized and graphitic domains is energetically favorable and kinetically accelerated at slightly elevated temperatures compared to room temperature. We demonstrate that such phase transformation processes have significant impact on the sheet properties by (1) making GO strongly absorbing in the visible, (2) reducing the electrical resistance by four orders of magnitude, and (3) shifting PL emission to the blue, without compromising the oxygen content. In addition to shedding light on the thermal stability of GO nanostructures when employed in devices operating above room temperature, these results open up novel opportunities for bulk processing of as-synthesized GO structures, and highlight pathways to tune the sheet properties of GO for their application in next-generation functional devices.

Using the phase transformation discovered, we demonstrate two different ap-

plications utilizing the same. First, we demonstrated enhanced cell capture efficiencies using mildly annealed GO compared to as-synthesized GO as substrates. Our results show that C-N functionalization and antibody grafting on to GO nano sheets are improved at the nanoscale through mild annealing and this is turn translates into enhanced cell capture capabilities at the macro scale. Second, our experimental and theoretical analyses suggest that rGO sheets with superior electrical characteristics can be fabricated by facilitating sp^2 (or oxygen) clustering in GO prior to its reduction. The present study is particularly important since the current practice to obtain rGO is to directly reduce as-synthesized GO films without incorporating any intermediate processing step, which is equivalent to the control sample in our experiments. Further, using atomistic simulations, we show enhanced oxygen and carbon removal upon oxygen clustering, which can be used to control the local residual oxygen content and pore formation in rGO. Our strategy could open up novel routes toward the production of rGO, synthesis of graphene quantum dots and development of graphene for membrane applications.

We would like to remark that, in this thesis, we study the structural organization happening in GO thin films which consists of at least ten monolayers. Observing structural transitions using transmission electron microscopy is an interesting challenge for the community of GO. This has not been addressed in this thesis and would be an important task for the future to confirm the clustering of oxygens at the nanoscale using such a direct evidence technique. Efforts in our group are being undertaken to accomplish this task. Another important thing to note is the role of amorphous carbons that are naturally deposited on the surface of GO monolayers. Although not studied in this thesis, this might play a role in dictating properties of GO monolayers. Finally, we believe that this work has

opened a new direction in the field of GO, since it is evident that we obtain a new and modified form of GO from our procedure. As a result, another interesting future task would be to look at new applications that be enabled based on these modified GO structures. We have shown two areas where it can make an impact, but exploring other areas could be potentially beneficial.

Bibliography

[1] A. Geim and K. Novoselov, "The rise of graphene (editorial)," *Nat. Mat.*, vol. 6, p. 183, 2007.

[2] Y. Zhu, S. Murali, W. Cai, X. Li, J. W. Suk, J. R. Potts, and R. S. Ruoff, "Graphene and graphene oxide: Synthesis, properties, and applications," *Advanced Materials*, vol. 22, no. 35, pp. 3906–3924, 2010.

[3] "http://www.graphenea.com/pages/graphene-properties,"

[4] S. Bae, H. Kim, Y. Lee, X. Xu, J.-S. Park, Y. Zheng, J. Balakrishnan, T. Lei, H. R. Kim, Y. I. Song, Y.-J. Kim, K. S. Kim, B. Ozyilmaz, J.-H. Ahn, B. H. Hong, and S. Iijima, "Roll-to-roll production of 30-inch graphene films for transparent electrodes," *Nature Nanotechnology*, vol. 5, no. 8, pp. 574–578, 2010.

[5] G. Eda and M. Chhowalla, "Chemically derived graphene oxide: Towards large-area thin-film electronics and optoelectronics," *Advanced Materials*, vol. 22, no. 22, pp. 2392–2415, 2010.

[6] K. P. Loh, Q. Bao, G. Eda, and M. Chhowalla, "Graphene oxide as a chemically tunable platform for optical applications.," *Nature chemistry*, vol. 2, no. 12, pp. 1015–1024, 2010.

[7] A. K. Geim, "Graphene: Status and prospects," *Science*, vol. 324, no. 5934, pp. 1530–1534, 2009.

[8] A. Bagri, C. Mattevi, M. Acik, Y. J. Chabal, M. Chhowalla, and V. B. Shenoy, "Structural evolution during the reduction of chemically derived graphene oxide.," *Nature chemistry*, vol. 2, no. 7, pp. 581–587, 2010.

[9] S. Stankovich, D. A. Dikin, G. H. B. Dommett, K. M. Kohlhaas, E. J. Zimney, E. A. Stach, R. D. Piner, S. T. Nguyen, and R. S. Ruoff, "Graphene-based composite materials.," *Nature*, vol. 442, no. 7100, pp. 282–286, 2006.

[10] S. Stankovich, D. Dikin, R. Piner, K. Kohlhaas, A. Kleinhammes, Y. Jia, Y. Wu, S. Nguyen, and R. Ruoff, "Synthesis of graphene-based nanosheets *via* chemical reduction of exfoliated graphite oxide," *Carbon*, vol. 45, no. 7, pp. 1558–1565, 2007.

[11] P. H. Wobkenberg, G. Eda, D.-S. Leem, J. C. De Mello, D. D. C. Bradley, M. Chhowalla, and T. D. Anthopoulos, "Reduced graphene oxide electrodes for large area organic electronics.," *Advanced materials Deerfield Beach Fla*, vol. 23, no. 13, pp. 1558–1562, 2011.

[12] A. Bagri, R. Grantab, N. V. Medhekar, and V. B. Shenoy, "Stability and formation mechanisms of carbonyl- and hydroxyl-decorated holes in graphene oxide," *The Journal of Physical Chemistry C*, vol. 114, no. 28, pp. 12053–12061, 2010.

[13] S. Pei and H.-M. Cheng, "The reduction of graphene oxide," *Carbon*, vol. 50, no. 9, pp. 3210 – 3228, 2012. Festschrift dedicated to Peter A. Thrower, Editor-in-Chief, 1972 - 2012.

[14] G. Eda, G. Fanchini, and M. Chhowalla, "Large-area ultrathin films of reduced graphene oxide as a transparent and flexible electronic material.," *Nature Nanotechnology*, vol. 3, no. 5, pp. 270–274, 2008.

[15] P. V. Kamat, "Meeting the clean energy demand: nanostructure architectures for solar energy conversion," *The Journal of Physical Chemistry C*, vol. 111, no. 7, pp. 2834–2860, 2007.

[16] R. K. Joshi, P. Carbone, F. C. Wang, V. G. Kravets, Y. Su, I. V. Grigorieva, H. A. Wu, A. K. Geim, and R. R. Nair, "Precise and ultrafast molecular sieving through graphene oxide membranes," *Science*, vol. 343, no. 6172, pp. 752–754, 2014.

[17] H. W. Kim, H. W. Yoon, S.-M. Yoon, B. M. Yoo, B. K. Ahn, Y. H. Cho, H. J. Shin, H. Yang, U. Paik, S. Kwon, J.-Y. Choi, and H. B. Park, "Selective gas transport through few-layered graphene and graphene oxide membranes," *Science*, vol. 342, no. 6154, pp. 91–95, 2013.

[18] H. Li, Z. Song, X. Zhang, Y. Huang, S. Li, Y. Mao, H. J. Ploehn, Y. Bao, and M. Yu, "Ultrathin, molecular-sieving graphene oxide membranes for selective hydrogen separation," *Science*, vol. 342, no. 6154, pp. 95–98, 2013.

[19] P. V. Kamat, "Graphene-based nanoassemblies for energy conversion," *The Journal of Physical Chemistry Letters*, vol. 2, no. 3, pp. 242–251, 2011.

[20] J.-M. Yun, J.-S. Yeo, J. Kim, H.-G. Jeong, D.-Y. Kim, Y.-J. Noh, S.-S. Kim, B.-C. Ku, and S.-I. Na, "Solution-processable reduced graphene oxide as a novel alternative to pedot:pss hole transport layers for highly efficient and stable polymer solar cells," *Adv. Mater.*, vol. 23, no. 42, pp. 4923–4928, 2011.

[21] B. Xu, S. Yue, Z. Sui, X. Zhang, S. Hou, G. Cao, and Y. Yang, "What is the choice for supercapacitors: Graphene or graphene oxide?," *Energy Environ. Sci.*, vol. 4, no. 8, pp. 2826–2830, 2011.

[22] X. Zhu, Y. Zhu, S. Murali, M. D. Stoller, and R. S. Ruoff, "Nanostructured reduced graphene oxide/fe2o3 composite as a high-performance anode material for lithium ion batteries," *ACS Nano*, vol. 5, no. 4, pp. 3333–3338, 2011.

[23] W. Gao, L. B. Alemany, L. Ci, and P. M. Ajayan, "New insights into the structure and reduction of graphite oxide.," *Nature chemistry*, vol. 1, no. 5, pp. 403–408, 2009.

[24] Z. Hossain, J. E. Johns, K. H. Bevan, H. J. Karmel, Y. T. Liang, S. Yoshimoto, K. Mukai, T. Koitaya, J. Yoshinobu, and M. Kawai, "*et al.* chemically homogeneous and thermally reversible oxidation of epitaxial graphene," *Nat. Chem.*, vol. 4, no. February, pp. 305–309, 2012.

[25] J. E. Johns and M. C. Hersam, "Atomic covalent functionalization of graphene," *Accounts of Chemical Research*, vol. 46, no. 1, pp. 77–86, 2013.

[26] W. S. Hummers and R. E. Offeman, "Preparation of graphitic oxide," *J. Am. Chem. Soc.*, vol. 80, no. 6, pp. 1339–1339, 1958.

[27] X. Gao, J. Jang, and S. Nagase, "Hydrazine and thermal reduction of graphene oxide: Reaction mechanisms, product structures, and reaction design," *The Journal of Physical Chemistry C*, vol. 114, no. 2, pp. 832–842, 2010.

[28] C. Mattevi, G. Eda, S. Agnoli, S. Miller, K. A. Mkhoyan, O. Celik, D. Mastrogiovanni, G. Granozzi, E. Garfunkel, and M. Chhowalla, "Evolution of electrical, chemical, and structural properties of transparent and conducting chemically derived graphene thin films," *Advanced Functional Materials*, vol. 19, no. 16, pp. 2577–2583, 2009.

[29] R. Larciprete, S. Fabris, T. Sun, P. Lacovig, A. Baraldi, and S. Lizzit, "Dual path mechanism in the thermal reduction of graphene oxide," *Journal of the American Chemical Society*, vol. 133, no. 43, pp. 17315–17321, 2011. PMID: 21846143.

[30] T. Sun, S. Fabris, and S. Baroni, "Surface precursors and reaction mechanisms for the thermal reduction of graphene basal surfaces oxidized by atomic oxygen," *The Journal of Physical Chemistry C*, vol. 115, no. 11, pp. 4730–4737, 2011.

[31] T. Sun and S. Fabris, "Mechanisms for oxidative unzipping and cutting of graphene," *Nano Letters*, vol. 12, no. 1, pp. 17–21, 2012. PMID: 22118714.

[32] D. R. Dreyer, S. Park, C. W. Bielawski, and R. S. Ruoff, "The chemistry of graphene oxide," *Chem. Soc. Rev.*, vol. 39, pp. 228–240, 2010.

[33] J. P. Rourke, P. A. Pandey, J. J. Moore, M. Bates, I. A. Kinloch, R. J. Young, and N. R. Wilson, "The real graphene oxide revealed: Stripping the oxidative

debris from the graphene-like sheets," *Angew. Chem. Int. Ed.*, vol. 50, no. 14, pp. 3173–3177, 2011.

[34] P. V. Kumar, M. Bernardi, and J. C. Grossman, "The impact of functionalization on the stability, work function, and photoluminescence of reduced graphene oxide," *ACS Nano*, vol. 7, no. 2, pp. 1638–1645, 2013.

[35] G. Eda, C. Mattevi, H. Yamaguchi, H. Kim, and M. Chhowalla, "Insulator to semimetal transition in graphene oxide," *The Journal of Physical Chemistry C*, vol. 113, no. 35, pp. 15768–15771, 2009.

[36] G. Eda, Y.-Y. Lin, C. Mattevi, H. Yamaguchi, H.-A. Chen, I.-S. Chen, C.-W. Chen, and M. Chhowalla, "Blue photoluminescence from chemically derived graphene oxide.," *Advanced materials*, vol. 22, no. 4, pp. 505–509, 2010.

[37] C.-T. Chien, S.-S. Li, W.-J. Lai, Y.-C. Yeh, H.-A. Chen, I.-S. Chen, L.-C. Chen, K.-H. Chen, T. Nemoto, and S. Isoda, "*et al.* tunable photoluminescence from graphene oxide.," *Angew. Chem. Int. Ed.*, vol. 51, pp. 6662–6666, 2012.

[38] S. Kim, S. Zhou, Y. Hu, M. Acik, Y. J. Chabal, C. Berger, W. De Heer, A. Bongiorno, and E. Riedo, "Room-temperature metastability of multilayer graphene oxide films.," *Nat. Mater.*, vol. 11, no. 6, pp. 544–549, 2012.

[39] J. T. Paci, T. Belytschko, and G. C. Schatz, "Computational studies of the structure, behavior upon heating, and mechanical properties of graphite oxide," *J. Phys. Chem. B*, vol. 111, no. 49, pp. 18099–18111, 2007.

[40] J.-A. Yan, L. Xian, and M. Y. Chou, "Structural and electronic properties of oxidized graphene," *Phys. Rev. Lett.*, vol. 103, p. 086802, Aug 2009.

[41] P. Johari and V. B. Shenoy, "Modulating optical properties of graphene oxide: role of prominent functional groups.," *ACS nano*, vol. 5, no. 9, pp. 7640–7, 2011.

[42] D. W. Boukhvalov and M. I. Katsnelson, "Modeling of graphite oxide.," *Journal of the American Chemical Society*, vol. 130, no. 32, pp. 10697–10701, 2008.

[43] S. Wang, P. K. Ang, Z. Wang, A. L. L. Tang, J. T. L. Thong, and K. P. Loh, "High mobility, printable, and solution-processed graphene electronics," *Nano Letters*, vol. 10, no. 1, pp. 92–98, 2010. PMID: 20025234.

[44] A. C. T. Van Duin, S. Dasgupta, F. Lorant, and W. A. Goddard, "Reaxff: A reactive force field for hydrocarbons," *J. Phys. Chem. A*, vol. 105, no. 41, pp. 9396–9409, 2001.

[45] R. Pentcheva, F. Wendler, H. L. Meyerheim, W. Moritz, N. Jedrecy, and M. Scheffler, "Jahn-teller stabilization of a "polar" metal oxide surface: $fe_3o_4(001)$," *Phys. Rev. Lett.*, vol. 94, p. 126101, Apr 2005.

[46] T. Szabo, O. Berkesi, P. Forgo, K. Josepovits, Y. Sanakis, D. Petridis, and I. Dekany, "Evolution of surface functional groups in a series of progressively oxidized graphite oxides," *Chem. Mater.*, vol. 18, no. 11, pp. 2740–2749, 2006.

[47] A. Hunt, D. A. Dikin, E. Z. Kurmaev, T. D. Boyko, P. Bazylewski, G. S. Chang, and A. Moewes, "Epoxide speciation and functional group distribution

in graphene oxide paper-like materials," *Adv. Funct. Mater.*, vol. 22, pp. 3950–3957, 2012.

[48] G. Henkelman, B. P. Uberuaga, and H. Jnsson, "A climbing image nudged elastic band method for finding saddle points and minimum energy paths," *The Journal of Chemical Physics*, vol. 113, no. 22, 2000.

[49] R. Zan, Q. M. Ramasse, U. Bangert, and K. S. Novoselov, "Graphene reknits its holes," *Nano Lett.*, vol. 12, no. 8, pp. 3936–3940, 2012.

[50] Z. Yin, S. Sun, T. Salim, S. Wu, X. Huang, Q. He, Y. M. Lam, and H. Zhang, "Organic photovoltaic devices using highly flexible reduced graphene oxide films as transparent electrodes.," *ACS nano*, vol. 4, no. 9, pp. 5263–5268, 2010.

[51] V. C. Tung, J.-H. Huang, I. Tevis, F. Kim, J. Kim, C.-W. Chu, S. I. Stupp, and J. Huang, "Surfactant-free water-processable photoconductive all-carbon composite," *J. Am. Chem. Soc.*, vol. 133, no. 13, pp. 4940–4947, 2011.

[52] Z. Wei, D. Wang, S. Kim, S. Y. Kim, Y. Hu, M. K. Yakes, A. R. Laracuente, Z. Dai, S. R. Marder, and C. Berger, "*et al.* nanoscale tunable reduction of graphene oxide for graphene electronics.," *Science*, vol. 328, no. 5984, pp. 1373–1376, 2010.

[53] S. Plimpton, "Fast parallel algorithms for short-range molecular dynamics," *J. Comput. Phys.*, vol. 117, pp. 1–19, 1995.

[54] G. Kresse and J. Furthmuller, "Efficient iterative schemes for ab-initio total-energy calculations using a plane-wave basis set.," *Phys. Rev. B*, vol. 54, no. 16, pp. 11169–11186, 1996.

[55] G. Kresse, "Efficiency of ab-initio total energy calculations for metals and semiconductors using a plane-wave basis set," *Comput. Mater. Sci.*, vol. 6, no. 1, pp. 15–50, 1996.

[56] G. Kresse and D. Joubert, "From ultrasoft pseudopotentials to the projector augmented-wave method," *Phys. Rev. B*, vol. 59, p. 1758, 1999.

[57] J. Perdew, K. Burke, and M. Ernzerhof, "Generalized gradient approximation made simple.," *Phys. Rev. Lett.*, vol. 77, no. 18, pp. 3865–3868, 1996.

[58] P. V. Kumar, S. Bardhan, Neelkanth M. andTongay, J. Wu, A. M. Belcher, and J. C. Grossman, "Scalable enhancement of graphene oxide properties by thermally driven phase transformation," *Nature Chemistry*, vol. 6, 2014.

[59] M.-T. Nguyen, R. Erni, and D. Passerone, "Two-dimensional nucleation and growth mechanism explaining graphene oxide structures," *Phys. Rev. B*, vol. 86, p. 115406, Sep 2012.

[60] M. Topsakal and S. Ciraci, "Domain formation on oxidized graphene," *Phys. Rev. B*, vol. 86, p. 205402, Nov 2012.

[61] B. Huang, H. Xiang, Q. Xu, and S.-H. Wei, "Overcoming the phase inhomogeneity in chemically functionalized graphene: The case of graphene oxides," *Phys. Rev. Lett.*, vol. 110, p. 085501, Feb 2013.

[62] K.-H. Liao, A. Mittal, S. Bose, C. Leighton, K. A. Mkhoyan, and C. W. Macosko, "Aqueous only route toward graphene from graphite oxide," *ACS Nano*, vol. 5, no. 2, pp. 1253–1258, 2011.

[63] H. Feng, R. Cheng, X. Zhao, X. Duan, and J. Li, "A low-temperature method to produce highly reduced graphene oxide," *Nature Commun.*, vol. 5, pp. 1539–1545, 2013.

[64] A. C. Ferrari and J. Robertson, "Interpretation of raman spectra of disordered and amorphous carbon," *Phys. Rev. B*, vol. 61, pp. 14095–14107, May 2000.

[65] M. Chhowalla, A. C. Ferrari, J. Robertson, and G. A. J. Amaratunga, "Evolution of sp2 bonding with deposition temperature in tetrahedral amorphous carbon studied by raman spectroscopy," *Applied Physics Letters*, vol. 76, no. 11, 2000.

[66] A. C. Ferrari, B. Kleinsorge, N. A. Morrison, A. Hart, V. Stolojan, and J. Robertson, "Stress reduction and bond stability during thermal annealing of tetrahedral amorphous carbon," *Journal of Applied Physics*, vol. 85, no. 10, 1999.

[67] X. Fan, W. Peng, Y. Li, X. Li, S. Wang, G. Zhang, and F. Zhang, "Deoxygenation of exfoliated graphite oxide under alkaline conditions: A green route to graphene preparation," *Advanced Materials*, vol. 20, no. 23, pp. 4490–4493, 2008.

[68] I. Jung, D. A. Dikin, R. D. Piner, and R. S. Ruoff, "Tunable electrical conductivity of individual graphene oxide sheets reduced at low temperatures," *Nano Lett.*, vol. 8, no. 12, pp. 4283–4287, 2008.

[69] L. Ci, L. Song, C. Jin, D. Jariwala, D. Wu, Y. Li, A. Srivastava, Z. F. Wang, K. Storr, L. Balicas, F. Liu, and P. M. Ajayan, "Atomic layers of hybridized boron nitride and graphene domains," *Nat. Mater.*, no. 5, pp. 430–435, 2010.

[70] P. Holliger and P. J. Hudson, "Engineered antibody fragments and the rise of single domains.," *Nature Biotechnology*, vol. 23, no. 9, pp. 1126 – 1136, 2005.

[71] S. Muyldermans, "Nanobodies: Natural single-domain antibodies," *Annual Review of Biochemistry*, vol. 82, no. 1, pp. 775–797, 2013. PMID: 23495938.

[72] H. J. Yoon, M. Kozminsky, and S. Nagrath, "Emerging role of nanomaterials in circulating tumor cell isolation and analysis," *ACS Nano*, vol. 8, no. 3, pp. 1995–2017, 2014. PMID: 24601556.

[73] H. J. Yoon, T. H. Kim, Z. Zhang, E. Azizi, T. M. Pham, C. Paoletti, J. Lin, N. Ramnath, M. S. Wicha, D. F. Hayes, D. M. Simeone, and S. Nagrath, "Sensitive capture of circulating tumour cells by functionalized graphene oxide nanosheets," *Nature Nanotechnology*, vol. 8, pp. 735–741, 10 2013. Date revised - 2014-11-01; Last updated - 2014-11-05.

[74] S. Wang, K. Liu, J. Liu, Z. T.-F. Yu, X. Xu, L. Zhao, T. Lee, E. K. Lee, J. Reiss, Y.-K. Lee, L. W. K. Chung, J. Huang, M. Rettig, D. Seligson, K. N. Duraiswamy, C. K.-F. Shen, and H.-R. Tseng, "Highly efficient capture of circulating tumor cells by using nanostructured silicon substrates with integrated chaotic micromixers," *Angewandte Chemie International Edition*, vol. 50, no. 13, pp. 3084–3088, 2011.

[75] "Isolation of rare circulating tumour cells in cancer patients by microchip technology.," *Nature*, vol. 450, no. 7173, pp. 1235 – 1239, 2007.

[76] O. C. Compton, D. A. Dikin, K. W. Putz, L. C. Brinson, and S. T. Nguyen, "Electrically conductive alkylated graphene paper via chemical reduction of amine-functionalized graphene oxide paper," *Advanced Materials*, vol. 22, no. 8, pp. 892–896, 2010.

[77] H. R. Thomas, A. J. Marsden, M. Walker, N. R. Wilson, and J. P. Rourke, "Sulfur-functionalized graphene oxide by epoxide ring-opening," *Angewandte Chemie International Edition*, vol. 53, no. 29, pp. 7613–7618, 2014.

[78] Y. Matsuo, T. Miyabe, T. Fukutsuka, and Y. Sugie, "Preparation and characterization of alkylamine-intercalated graphite oxides," *Carbon*, vol. 45, no. 5, pp. 1005 – 1012, 2007.

[79] H. Zhu, M. Zhang, S. Cai, Y. Cai, P. Wang, S. Bao, M. Zou, and M. Du, "In situ growth of rh nanoparticles with controlled sizes and dispersions on the cross-linked pva-pei nanofibers and their electrocatalytic properties towards h2o2," *RSC Adv.*, vol. 4, pp. 794–804, 2014.

[80] C. Gomez-Navarro, R. T. Weitz, A. M. Bittner, M. Scolari, A. Mews, M. Burghard, and K. Kern, "Electronic transport properties of individual chemically reduced graphene oxide sheets," *Nano Letters*, vol. 7, no. 11, pp. 3499–3503, 2007. PMID: 17944526.

[81] D. Cohen-Tanugi and J. C. Grossman, "Water desalination across nanoporous graphene," *Nano Letters*, vol. 12, no. 7, pp. 3602–3608, 2012. PMID: 22668008.

[82] D.-e. Jiang, A. C. T. van Duin, W. A. Goddard, and S. Dai, "Simulating the initial stage of phenolic resin carbonization via the reaxff reactive force field,"

The Journal of Physical Chemistry A, vol. 113, no. 25, pp. 6891–6894, 2009. PMID: 19496580.

[83] C. W. Bauschlicher, T. Qi, E. J. Reed, A. Lenfant, J. W. Lawson, and T. G. Desai, "Comparison of reaxff, dftb, and dft for phenolic pyrolysis. 2. elementary reaction paths," *The Journal of Physical Chemistry A*, vol. 117, no. 44, pp. 11126–11135, 2013. PMID: 24093151.

[84] T. Qi, C. W. Bauschlicher, J. W. Lawson, T. G. Desai, and E. J. Reed, "Comparison of reaxff, dftb, and dft for phenolic pyrolysis. 1. molecular dynamics simulations," *The Journal of Physical Chemistry A*, vol. 117, no. 44, pp. 11115–11125, 2013. PMID: 24094313.